

MEASUREMENT OF ACOUSTIC GLITCHES IN SOLAR-TYPE STARS
 FROM OSCILLATION FREQUENCIES OBSERVED BY *Kepler*

A. MAZUMDAR¹, M. J. P. F. G. MONTEIRO^{2,3}, J. BALLOT^{4,5}, H. M. ANTIA⁶, S. BASU⁷, G. HOUDEK^{8,9}, S. MATHUR^{10,15},
 M. S. CUNHA², V. SILVA AGUIRRE^{8,11}, R. A. GARCÍA¹², D. SALABERT¹³, G. A. VERNER¹⁴, J. CHRISTENSEN-DALSGAARD⁸,
 T. S. METCALFE^{15,8}, D. T. SANDERFER¹⁶, S. E. SEADER¹⁷, J. C. SMITH¹⁷, W. J. CHAPLIN¹⁴

Draft version December 18, 2013

ABSTRACT

For the very best and brightest asteroseismic solar-type targets observed by *Kepler*, the frequency precision is sufficient to determine the acoustic depths of the surface convective layer and the helium ionization zone. Such sharp features inside the acoustic cavity of the star, which we call acoustic glitches, create small oscillatory deviations from the uniform spacing of frequencies in a sequence of oscillation modes with the same spherical harmonic degree. We use these oscillatory signals to determine the acoustic locations of such features in 19 solar-type stars observed by the *Kepler* mission. Four independent groups of researchers utilized the oscillation frequencies themselves, the second differences of the frequencies and the ratio of the small and large separation to locate the base of the convection zone and the second helium ionization zone. Despite the significantly different methods of analysis, good agreement was found between the results of these four groups, barring a few cases. These results also agree reasonably well with the locations of these layers in representative models of the stars. These results firmly establish the presence of the oscillatory signals in the asteroseismic data and the viability of several techniques to determine the location of acoustic glitches inside stars.

Subject headings: stars: oscillations — stars: interiors

1. INTRODUCTION

Acoustic glitches in a star are the regions where the sound speed undergoes an abrupt variation due to a localized sharp change in the stratification. The major acoustic glitches are the boundaries between radiative and convective regions and the layers of ionization of elements, especially hydrogen and helium. Such a glitch introduces an oscillatory component, $\delta\nu$, in the eigenfrequencies of the star with respect to the frequencies themselves (Gough & Thompson 1988; Vorontsov

1988; Gough 1990), proportional to

$$\delta\nu \propto \sin(4\pi\tau_g\nu_{n,l} + \phi), \quad (1)$$

where

$$\tau_g = \int_{r_g}^{R_s} \frac{dr}{c}, \quad (2)$$

is the acoustic depth of the glitch measured from the surface, c the adiabatic sound speed, r_g the radial distance of the glitch, R_s the seismic radius of the star (see discussion below), $\nu_{n,l}$ the frequency of a mode with radial order n and degree l , and ϕ a phase factor. Each glitch will contribute to such a signal in the frequencies with a “periodicity” of twice the acoustic depth of the corresponding glitch.

This oscillatory signature has been extensively studied for the Sun in order to determine the extent of overshoot below the solar convection zone (Vorontsov 1988; Gough 1990; Gough & Sekii 1993; Monteiro et al. 1994; Basu et al. 1994; Roxburgh & Vorontsov 1994; Basu 1997; Christensen-Dalsgaard et al. 2011) and the seismic solar age (Houdek & Gough 2011).

It has been proposed earlier that this may be used for distant stars also to find the position of the base of the convective envelope or the second helium ionization zone (Monteiro et al. 2000; Mazumdar & Antia 2001; Gough 2002; Roxburgh & Vorontsov 2003; Ballot et al. 2004; Basu et al. 2004; Houdek 2004; Mazumdar 2005; Piau et al. 2005; Houdek & Gough 2006, 2007). Indeed, Miglio et al. (2010) have used the modulation of the frequency separations to determine the location of the second helium ionization zone in the red giant star, HR7349, observed with the *CoRoT* satellite. Recently, Mazumdar et al. (2012) have used the oscillatory signal in the second differences of the frequencies of the solar-type *CoRoT* target star HD49933 to determine the acoustic depths of its second helium ionization zone and the base of the convective envelope (see also Mazumdar et al.

¹ Homi Bhabha Centre for Science Education, TIFR, V. N. Purav Marg, Mankhurd, Mumbai 400088, India

² Centro de Astrofísica da Universidade do Porto, Rua das Estrelas, 4150-762 Porto, Portugal

³ Departamento de Física e Astronomia, Faculdade de Ciências da Universidade do Porto, Rua do Campo Alegre, 4169-007 Porto, Portugal

⁴ CNRS, Institut de Recherche en Astrophysique et Planétologie, 14 avenue Edouard Belin, 31400 Toulouse, France

⁵ Université de Toulouse, UPS-OMP, IRAP, 31400 Toulouse, France

⁶ Tata Institute of Fundamental Research, Homi Bhabha Road, Mumbai 400005, India

⁷ Astronomy Department, Yale University, P.O. Box 208101, New Haven, CT 065208101, USA

⁸ Stellar Astrophysics Centre, Department of Physics and Astronomy, Aarhus University, Ny Munkegade 120, DK-8000 Aarhus C, Denmark

⁹ Institute of Astronomy, University of Vienna, 1180, Vienna, Austria

¹⁰ High Altitude Observatory, NCAR, P.O. Box 3000, Boulder, CO 80307, USA

¹¹ Max Planck Institut für Astrophysik, Karl-Schwarzschild-Str. 1, 85748, Garching bei München, Germany

¹² Laboratoire AIM, CEA/DSM, CNRS, Université Paris Diderot, IRFU/SAP, Centre de Saclay, 91191 Gif-sur-Yvette Cedex, France

¹³ Laboratoire Lagrange, UMR7293, Université de Nice Sophia-Antipolis, CNRS, Observatoire de la Côte d’Azur, 06304 Nice, France

¹⁴ School of Physics and Astronomy, University of Birmingham, Edgbaston, Birmingham, B15 2TT, UK

¹⁵ Space Science Institute, Boulder, CO 80301, USA

¹⁶ NASA Ames Research Center, Moffett Field, CA 94035, USA

¹⁷ SETI Institute/NASA Ames Research Center, Moffett Field, CA 94035, USA

2011; Roxburgh 2011). Earlier, Bedding et al. (2010) reported detection of an acoustic glitch in Procyon, although no association to a specific layer was made.

The scientific interest in studying the acoustic glitches goes beyond the obvious goal of placing constraints on the positions of specific layers in the stellar interior. The accurate determination of the location and profile of the transition at the base of the convective envelope, for example, will help us refine our understanding of the stellar dynamo in cool stars. On the other hand, the amplitude of the oscillatory signal from the ionization zones is directly related to the abundance of the corresponding element in the star. For helium especially, an estimate of the helium abundance in an ensemble of stars of different masses and ages will lead us to a better understanding of the process of element enrichment in stars which can be extrapolated back to the primordial helium content of the universe, an important parameter in cosmology.

The acoustic glitches can be used to determine the acoustic depth of the surface convection zone in a star, which in turn can be used to constrain the stellar models. In particular, the position of the base of the convection zone is very sensitive to opacity of stellar material, which depends on the heavy element abundances. It is well known that the recent determination of heavy element abundances (Asplund et al. 2009) using 3D hydrodynamic atmospheric models for the Sun are not consistent with helioseismic data (Basu & Antia 2008; Gough 2013, and references therein). On the other hand, the older abundances of Grevesse & Sauval (1998) estimated using 1D atmospheric models are consistent with helioseismic data. The cause of this discrepancy is not understood and it would be interesting to test if asteroseismic data are consistent with the revised abundances. In particular, the heavy element abundance, Z , for stars is estimated from observed $[\text{Fe}/\text{H}]$ ratio. Thus the estimated value of Z depends on the heavy element mixture (ratio of Fe to H abundance) for the Sun. Recently van Saders & Pinsonneault (2012), noting the dependence on Z of the acoustic depth of the convection zone, proposed that the measured acoustic depth can be used to constrain Z .

The effects of the acoustic glitches are subtle, and hence great care is required in ascertaining that the results of the analyses reflect the stellar properties at a significant level. Although analysis of artificial data (e.g., Basu et al. 2004; Mazumdar 2005; Monteiro & Thompson 2005; Houdek & Gough 2007) are useful in this regard, real data may well give rise to effects that are not contained in such simulations. Here we test the reliability of the inferences by comparing the results of several independent fits to the glitch properties of the same frequency data, using rather different techniques. These all provide measures of the acoustic locations of the glitches which can be directly compared. Other properties of the fits, however, depend more sensitively on the techniques and hence can only properly be interpreted in the context of comparisons with model results. We return to this point in Sect. 6.

In the present analysis we studied 19 stars continuously observed by the *Kepler mission* (Borucki et al. 2010; Koch et al. 2010) during 9 months. Launched on 2009 March 7, *Kepler* is monitoring 150 000 stars in the constellations of Cygnus and Lyra every half an hour to look for Earth-like planets orbiting around solar-like stars. Photometric time series of a subsample of 512 stars are studied at a shorter cadence of 58.8 s (Gilliland et al. 2010). Every 3 months the spacecraft rolls by 90° , to maintain the solar panels directed towards the

Sun. Therefore, the datasets are organized in quarters. The time series of our sample of 19 stars were acquired during quarters 5 to 9, processed following the methods described by García et al. (2011), and their frequencies extracted as described by Appourchaux et al. (2012).

It must be noted that for the purpose of detection of the acoustic glitches, it is sufficient to tag the frequencies only by their angular degree, l . A visual inspection of the power spectrum yields a clear identification of l of the different modes. We do not need to know the absolute overtone number, n , of the modes. We only need to ensure that we do not have any “missing” orders (since the large separation, i.e., the average difference in frequency between successive overtones of the same angular degree l , is known from the power spectrum itself, this is a trivial step). Thus, when combining the frequencies to construct the required diagnostics, if the angular degree is known, the correct combination of frequencies can be made (in some cases that just means taking differences of frequencies of modes of the same degree). The methods that we describe in the next section are, therefore, independent of any input from stellar models which are usually used to identify the radial order of observed modes.

The choice of the sample of stars is only guided by the fact that these were among the stars with the best signal to noise ratio in the *Kepler* data. All the stars are classified as being either in the main sequence or early sub-giant phase and thus have very few mixed modes. Mixed modes hinder the detection of the oscillatory signal of the acoustic glitches, and are best avoided for the present purpose. There would be other similar stars in the same region of the HR diagram, which are also expected to exhibit similar signals of acoustic glitches; this is merely a random sample.

In the next section we describe in detail the different techniques used to determine the locations of the acoustic glitches. In Sect. 3 we present the acoustic locations resulting from our fits to the observed frequencies, while Sect. 4 compares them with analyses of associated stellar models. Sect. 5 provides a discussion of results for individual stars. We summarize the conclusions in Sect. 6. Appendix A presents details on the individual techniques, whereas Appendix B provides details of the stellar models used.

2. THE TECHNIQUES

We applied four different methods (labelled A to D in Appendix A) to determine the acoustic locations of the base of the convective zone (BCZ) and the second helium ionization zone (HeIIZ). The different methods were applied to the same input data, namely the *Kepler* frequencies of the stars, by different subsets of the present authors independently, and the final results are compared in Sec. 3.

The first method (Method A) utilizes the oscillatory signals in the frequencies themselves. Method B fits a functional form to the second differences of the frequencies with respect to the radial order with acoustic depths of BCZ and HeIIZ among the free parameters. Method C fits the second differences of the model frequency perturbations due to the glitches to the observed second differences. Lastly, method D utilizes the oscillatory signal present in the ratio of the small to the large separation. The large separation is the average difference in frequencies of same degree and successive radial order, while the small separation is the difference in frequency between a radial mode and the quadrupole mode of the previous radial order. Methods A, B, and C determine the acoustic depths (measured from the surface) of the BCZ and HeIIZ

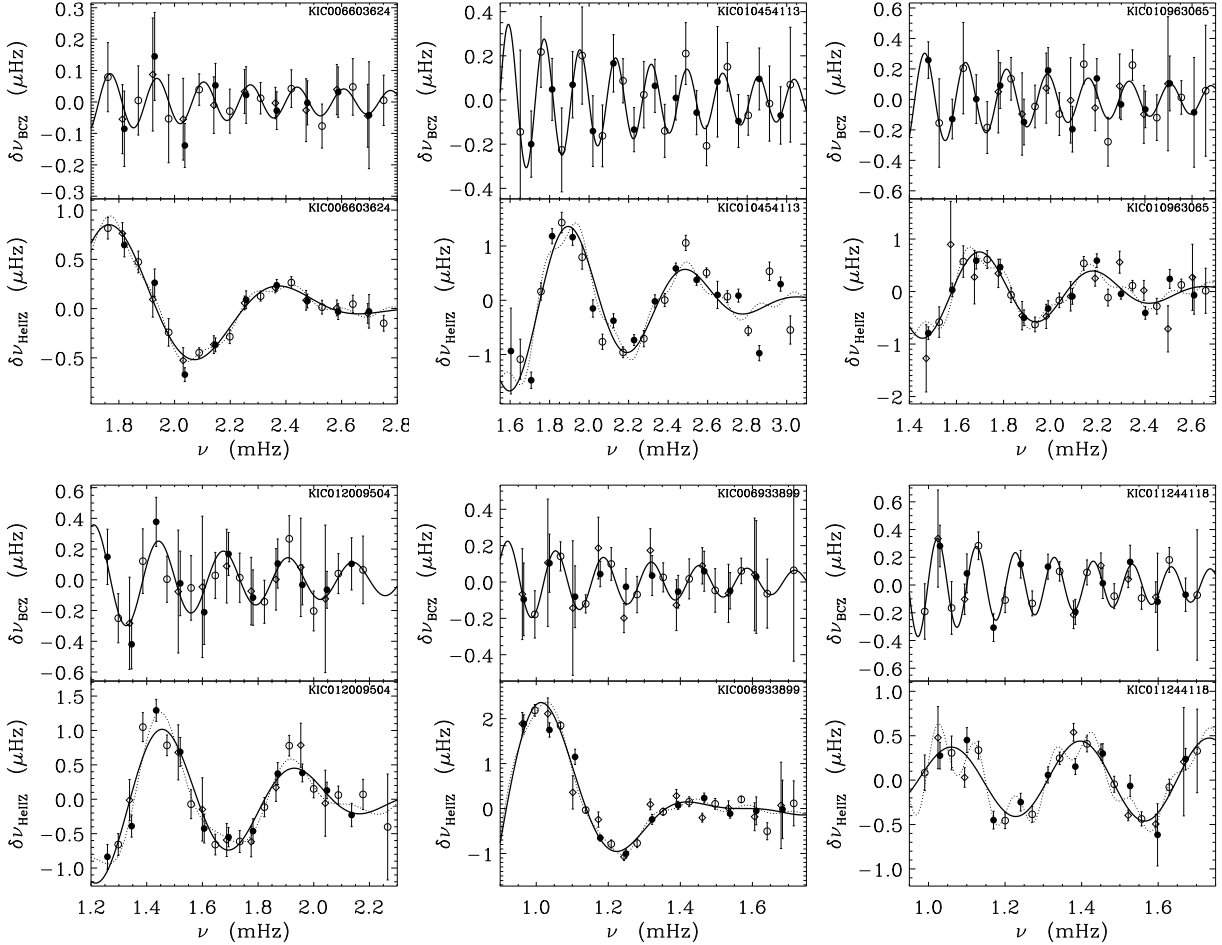


FIG. 2.— Illustration of method A: Fits of Eqs. (A1) and (A2) to the residuals of frequencies of six *Kepler* stars (KIC numbers given in each panel) after removing a smooth component iteratively. The points correspond to $l = 0$ (black circles), $l = 1$ (open circles) and $l = 2$ (diamonds). The *solid line* is the best fit to the BCZ component (Eq. (A1), *upper panel* for each star) and the HeIIz component (Eq. (A2), *lower panel* for each star). In the *lower panels* the dotted line shows the BCZ component superimposed on the HeIIz component, as obtained separately and shown in the upper panel.

stars are given in Table 1. The effective temperatures were adopted from Bruntt et al. (2012) while the $\log g$ values were determined from a seismic pipeline (Basu et al. 2010). The positions of the 19 stars on the Hertzsprung-Russell diagram are shown in Fig. 1. We show the results from each method graphically in Figs. 2, 3, 4 and 5 for a selected set of eight stars: KIC008006161, KIC006603624, KIC010454113, KIC010963065, KIC004914923, KIC012009504, KIC006933899, and KIC011244118. However, for methods A and D, not all the cases led to significant results for acoustic depths or radii of BCZ and HeIIz.

We compare the results for all the 19 stars from all four methods in Table 2. The acoustic radii of the BCZ (T_{BCZ}) determined by method D have been converted to acoustic depths (τ_{BCZ}) through the relation $\tau_{BCZ} = T_0 - T_{BCZ} = (2\Delta_0)^{-1} - T_{BCZ}$ for comparison with the values determined by other methods. However, the uncertainties quoted for τ_{BCZ} from method D are the intrinsic uncertainties from the method, and do not include the uncertainties in T_0 . Method D did not consider the presence of the HeIIz signal in the data.

In Fig. 6 we show the values of the acoustic depths obtained by different methods for all the stars. A detailed comparison of the results follows in Sect. 5.1.

4. COMPARISON WITH STELLAR MODELS

The acoustic locations of the glitches determined by all the methods described above do not depend on detailed modeling of the stars; they were derived purely from the observed frequencies. In order to check whether the estimated values of τ_{BCZ} and τ_{HeIIz} are consistent with typical stellar models, we compared them with values from representative models of each star. In this, we adopted two approaches. The first one consisted of comparing the values with a broad family of models constructed to match the average seismic and spectroscopic properties of the stars to a fair extent. Additionally, we compared our values with the theoretical values of one optimally fitted model for each star.

For this exercise, we compared not the acoustic depths directly, but the fractional acoustic radii of the BCZ and the HeIIz. This was done for two reasons. Firstly, in a stellar model the acoustic radius of a glitch, being calculated from the centre outwards, is relatively free from the poorly known contribution to the sound speed from the outermost layers of the stars which lie above the glitch. Thus it should be theoretically a more robust quantity than the acoustic depth, which, being calculated from the surface inwards would include the sound speed profile in the outer layers. However, in converting the acoustic depth estimated from the oscillatory signal in frequencies to the corresponding acoustic radius we do use the approximate relationship between the total acoustic ra-

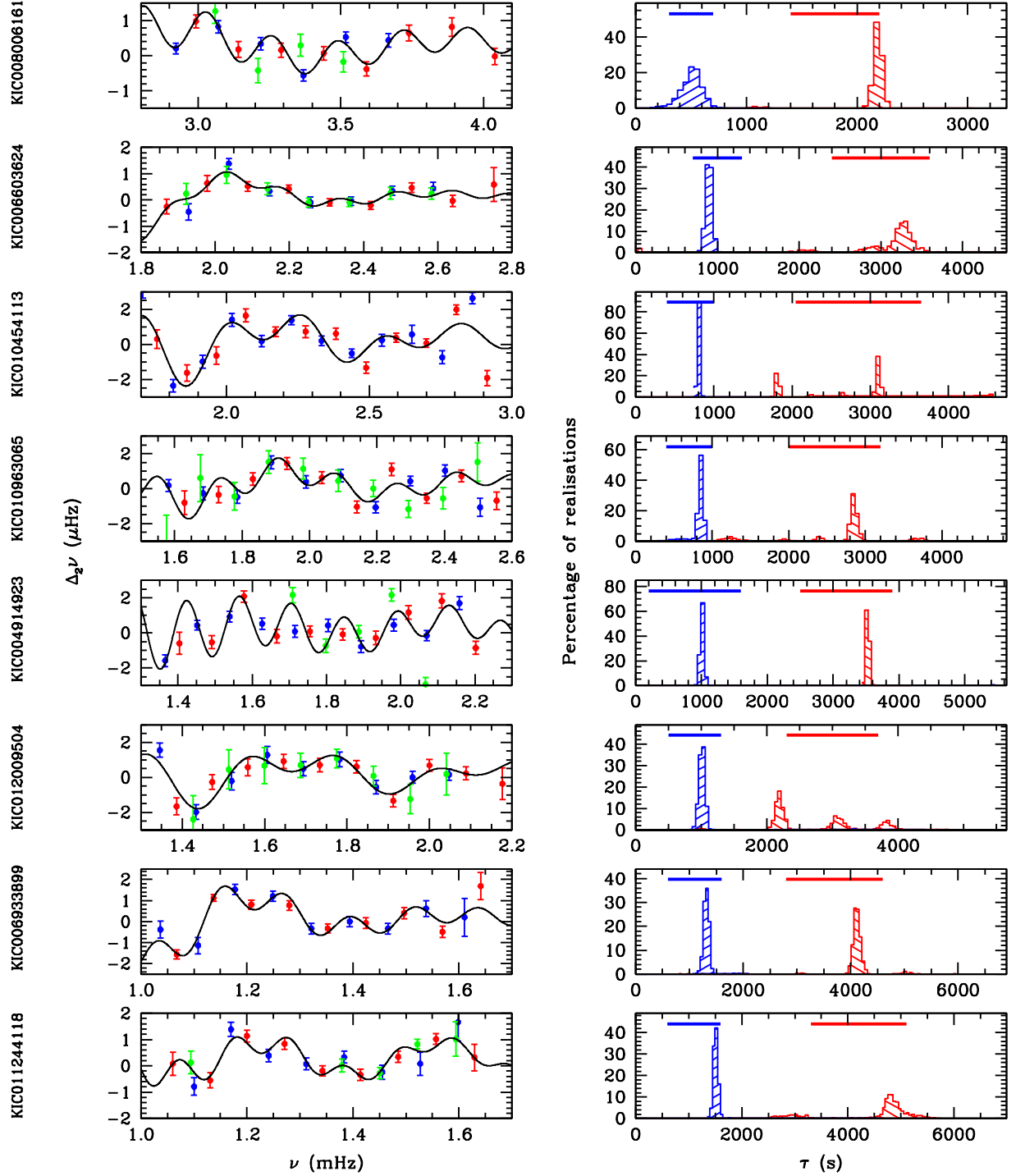


FIG. 3.— Illustration of method B: Fits of Eq. (A6) to the second differences of the mean frequencies for eight *Kepler* stars (KIC numbers on the *extreme left*) and the histograms for the fitted values of τ_{HeIz} and τ_{BCZ} for different realizations of the data. The second differences of the frequencies of $l=0$ (blue), $l=1$ (red) and $l=2$ (green) modes of the stars and their fit to Eq. (A6) (black curve) are shown in the *left panels*. The corresponding histograms of the fitted values of τ_{BCZ} (in red) and τ_{HeIz} (in blue) for different realizations are shown in the *right panels*. The *solid bands* at the top of the *right panels* indicate the range of initial guesses for the two parameters in each fit.

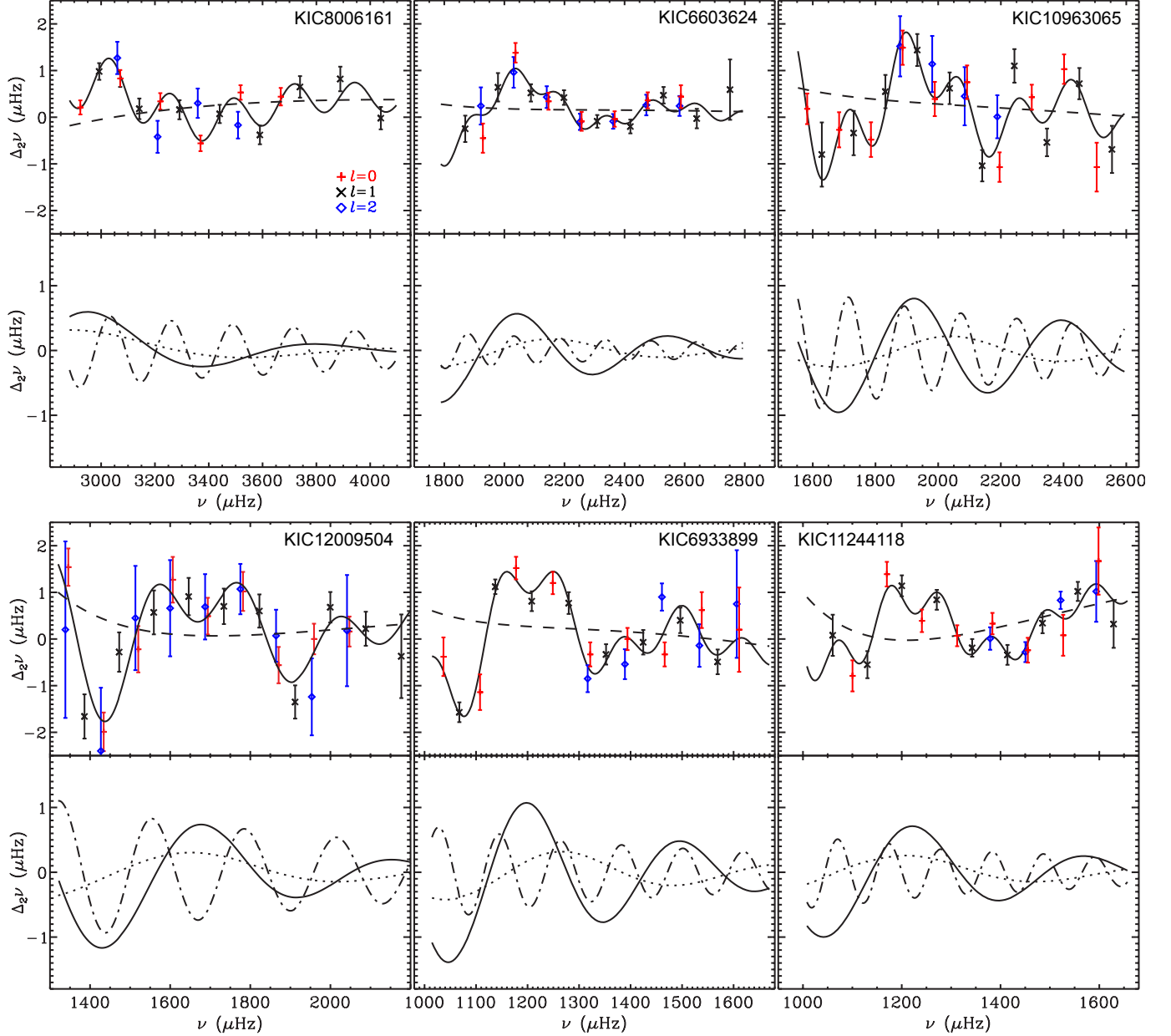


FIG. 4.— Illustration of method C: Analyses results for six *Kepler* stars (KIC numbers given in each panel). The symbols in the *upper panels* denote second differences $\Delta_2\nu$ for low-degree modes. The solid curves are fits to $\Delta_2\nu$ based on the analysis by Houdek & Gough (2007, 2011). The dashed curves are the smooth contributions, including a third-order polynomial in ν_i^{-1} to represent the upper-glitch contribution from near-surface effects. The *lower panels* display the remaining individual contributions from the acoustic glitches to $\Delta_2\nu$: the *dotted* and *solid* curves are the contributions from the first and second stages of helium ionization, and the *dot-dashed* curve is the contribution from the acoustic glitch at the base of the convective envelope.

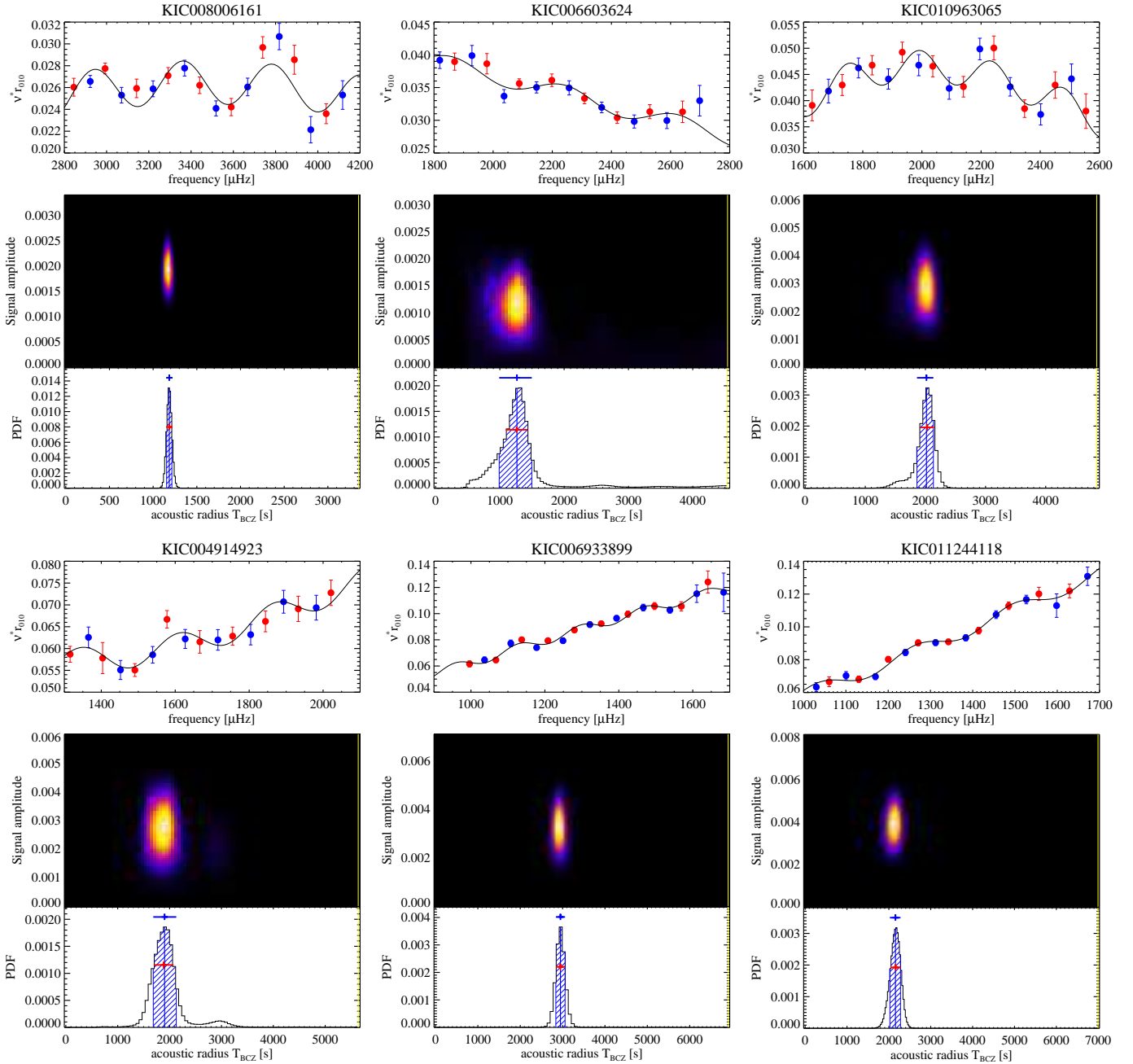


FIG. 5.— Illustration of method D: Determination of T_{BCZ} using frequency ratios for six *Kepler* targets. Each of the six panels corresponds to a target and is divided into three sub-panels. *Top* sub-panels show the seismic variables $\nu^* r_{010}$. *Blue (red)* dots with error bars are the observed values for $\nu^* r_{010}$ ($\nu^* r_{10}$). *Solid lines* show models (Eq. (A19)) with the parameters corresponding to the highest posterior probabilities found by MCMC. *Middle* sub-panels are 2-D probability functions in the plane (T, A) . *White (black)* color corresponds to high (low) probability. *Bottom* sub-panels show marginal probability distributions for the parameter T . Vertical *blue* lines indicate the medians of the distributions and hatched areas show the 68%-level confidence intervals. *Blue* error bars, plotted above the peaks, are uncertainties deduced from these intervals, whereas *red* uncertainties, plotted across the peaks, are obtained by fitting the peaks with Gaussian profiles.

dus and the large separation. Secondly, by considering the fractional acoustic radii instead of the acoustic radii itself, we remove the effect of overall homology scaling of the models at slightly different masses and radii. Of course, the shift between the models in the relative position of the BCZ and the HeIIZ inside the star reflects a true departure of the models from the observed star.

4.1. Neighborhood models

In this approach, we considered a broad family of theoretical models which mimic the global properties of the stars and their seismic properties, as listed in Table 1, but cannot be claimed to necessarily have frequencies that match the observed ones very closely. We deliberately spanned a very broad range in each of the global properties. This is because our aim here was to only determine the possible range in the locations of the acoustic glitches in stellar models similar to the target star, and compare the values estimated from the *Ke-*

TABLE 2
COMPARISON OF ACOUSTIC DEPTHS OF THE BASE OF THE CONVECTIVE ENVELOPE (τ_{BCZ}) AND THE SECOND HELIUM IONIZATION ZONE (τ_{HeIIz}) BY FOUR INDEPENDENT METHODS.

KIC ID	T_0 (s)	τ_{BCZ} (s)				τ_{HeIIz} (s)		
		Method A	Method B	Method C	Method D	Method A	Method B	Method C
KIC008006161*	3353 \pm 2	2284 ⁺⁴⁷ ₋₄₇	2186 ⁺³⁵ ₋₃₉	2199 ⁺⁴⁰ ₋₃₈	2169 ⁺³⁰ ₋₃₀	...	508 ⁺⁸⁰ ₋₁₀₁	615 ⁺¹²³ ₋₁₄₄
KIC008379927	4170 \pm 3	1796 ⁺¹¹⁴ ₋₁₁₄	1840 ⁺²⁹ ₋₂₆	1858 ⁺⁴⁰ ₋₃₈	(3172 ⁺⁶¹)	...	714 ⁺²⁵ ₋₂₇	827 ⁺⁴⁸ ₋₅₇
KIC008760414	4273 \pm 3	2750 ⁺¹³² ₋₁₃₂	2481 ⁺³¹⁶ ₋₁₀₀	...	2430 ⁺¹⁴¹ ₋₁₄₁	...	973 ⁺⁸² ₋₁₈₅	...
KIC006603624*	4549 \pm 4	2932 ⁺¹⁸³ ₋₁₈₃	3234 ⁺¹³³ ₋₄₃₈	3285 ⁺¹³⁰ ₋₁₉₆	3287 ⁺¹⁷¹ ₋₁₇₁	829 ⁺⁸⁹ ₋₈₉	897 ⁺³⁶ ₋₃₇	1031 ⁺⁶¹ ₋₉₆
KIC010454113*	4757 \pm 9	2801 ⁺¹²⁵ ₋₁₂₅	3083 ⁺³³ ₋₁₅₄	3126 ⁺⁷⁵ ₋₁₂₂	...	823 ⁺¹⁸ ₋₁₈	804 ⁺¹³ ₋₁₅	840 ⁺⁷ ₋₈
KIC006106415	4821 \pm 4	2903 ⁺²⁴² ₋₂₄₂	2875 ⁺³⁹³ ₋₂₄₇	...	2811 ⁺¹¹⁸ ₋₁₁₈	...	908 ⁺⁷⁴ ₋₇₅	...
KIC010963065*	4882 \pm 4	2832 ⁺¹⁵⁵ ₋₁₅₅	2854 ⁺⁴⁷ ₋₄₂	2803 ⁺¹²⁰ ₋₁₆₆	2852 ⁺¹¹² ₋₁₁₂	1020 ⁺⁶² ₋₆₂	851 ⁺²⁴ ₋₂₄	1101 ⁺²⁷ ₋₂₉
KIC006116048	4985 \pm 9	3153 ⁺²²⁰ ₋₂₂₀	2942 ⁺¹⁷⁸ ₋₂₇₃	3003 ⁺¹⁴¹ ₋₃₄₇	3134 ⁺¹⁸⁶ ₋₁₈₆	1015 ⁺¹⁰⁸ ₋₁₀₈	1048 ⁺³⁴ ₋₃₅	1094 ⁺¹¹ ₋₉₂
KIC004914923*	5662 \pm 6	3744 ⁺⁹¹ ₋₉₁	3525 ⁺²³ ₋₂₁	3526 ⁺²³ ₋₂₉	3777 ⁺¹⁹¹ ₋₁₉₁	...	1006 ⁺²³ ₋₂₅	1151 ⁺⁷ ₋₅₆
KIC012009504*	5701 \pm 6	2150 ⁺⁷⁴ ₋₇₄	2174 ⁺⁹⁰ ₋₂₈₈	2192 ⁺⁸⁴ ₋₁₀₃	...	1039 ⁺⁴⁷ ₋₄₇	1004 ⁺⁴⁰ ₋₄₇	1089 ⁺¹² ₋₆₆
KIC012258514	6711 \pm 9	2645 ⁺¹⁵¹ ₋₁₅₁	2819 ⁺¹⁷³ ₋₃₃₈	1277 ⁺⁸¹ ₋₈₁	1250 ⁺⁶⁷ ₋₇₈	...
KIC006933899*	6963 \pm 9	3773 ⁺²⁰¹ ₋₂₀₁	4115 ⁺⁷⁴ ₋₆₅	4228 ⁺⁶⁷⁵ ₋₁₄₃	4014 ⁺¹⁰⁷ ₋₁₀₇	1114 ⁺¹²⁴ ₋₁₂₄	1315 ⁺⁵⁴ ₋₄₅	1721 ⁺⁷⁷ ₋₆₄
KIC011244118*	7012 \pm 19	4829 ⁺²⁵¹ ₋₂₅₁	4844 ⁺²⁴⁶ ₋₁₃₃	4798 ⁺¹⁶⁵ ₋₅₇₆	4851 ⁺¹²⁵ ₋₁₂₅	1490 ⁺⁴⁰ ₋₄₀	1506 ⁺⁴¹ ₋₃₃	1501 ⁺⁸⁸ ₋₁₃₂
KIC008228742	8116 \pm 13	4409 ⁺²⁹⁰ ₋₂₉₀	4468 ⁺⁸⁹ ₋₁₆₆	...	4565 ⁺¹⁸⁷ ₋₁₈₇	...	1509 ⁺³⁸ ₋₄₆	...
KIC003632418	8264 \pm 13	5199 ⁺¹²⁴ ₋₁₂₄	5124 ⁺¹⁹⁵ ₋₁₄₉	...	5062 ⁺¹⁷³ ₋₁₇₃	...	1462 ⁺⁶⁹ ₋₇₈	...
KIC010018963	9057 \pm 32	5137 ⁺³¹⁰ ₋₃₁₀	3820 ⁺²⁴⁴ ₋₃₅₇	1972 ⁺⁵⁵ ₋₅₆	...
KIC007976303	9823 \pm 38	7026 ⁺³⁵ ₋₃₅	6760 ⁺⁷⁵ ₋₈₀	2835 ⁺⁵¹ ₋₅₁	2671 ⁺³³ ₋₃₀	...
KIC011026764	9960 \pm 19	5053 ⁺³³ ₋₃₃	5048 ⁺⁴³ ₋₃₈	2316 ⁺⁶⁶ ₋₇₂	...
KIC011395018	10548 \pm 22	6504 ⁺²⁷⁶ ₋₂₇₆	7223 ⁺⁶⁰ ₋₅₇	3592 ⁺⁴⁰ ₋₃₈	...

¹ In method D actually the acoustic *radius*, T_{BCZ} was determined, which has been converted to the corresponding acoustic *depth*, τ_{BCZ} using the T_0 value derived from the average large separation, Δ_0 .

² A blank cell indicates that an estimation of the acoustic depth was not attempted, and a cell with ... indicates that the estimated value did not pass the applied validity check for the relevant method.

³ Values in parentheses denote a significant detection, but not associated with an acoustic glitch.

⁴ For KIC010454113 a secondary value of $\tau_{\text{BCZ}} \approx 1850$ s is obtained with lesser significance than the value quoted in methods B and C.

* Stars illustrated in Figs. 2–5.

pler data. Further, we repeated the exact procedure of one of the methods (B) to obtain the acoustic depths τ_{BCZ} and τ_{HeIIz} from the theoretical frequencies of the stellar models. This allowed us also to investigate possible systematic shifts between the theoretical acoustic locations of the glitches from the models and their estimated values from the oscillatory signal in the model frequencies themselves.

We used the Yale Stellar Evolution Code (YREC; Demarque et al. 2008) to model the stars. A detailed description of the models can be found in Appendix B. The first step of our modeling was to use the average large separation Δ_0 and the frequency of maximum power, ν_{max} , along with T_{eff} and metallicity to determine the masses of the stars using a grid-based Yale-Birmingham pipeline (Basu et al. 2010; Gai et al. 2011). Mathur et al. (2012) have shown that grid-based estimates of stellar masses and radii agree very well with those obtained from more detailed modeling of the oscillation frequencies of stars, though with slightly lower precision (see also Silva Aguirre et al. 2011).

For each star, we specified 8–12 initial masses scanning a 2σ range on either side of the mass obtained by the grid modeling. For each initial mass we modelled the star using three values of the mixing length parameter α (1.826, 1.7 and 1.5; note $\alpha = 1.826$ is the solar calibrated value of α for YREC). For each value of mass and α we assumed at least four different values of the initial helium abundance Y_0 . In general Y_0 ranged from 0.25 to 0.30. The models were evolved from ZAMS and the properties were output at short intervals to allow us to calculate oscillation frequencies for the model as it evolved.

All models satisfying the observed constraints on large sep-

aration, small separation, T_{eff} , $\log g$ and $[\text{Fe}/\text{H}]$ were selected for comparison. In order to get a reasonably large number of models the uncertainty margin was assumed to be $2.0 \mu\text{Hz}$, $2.0 \mu\text{Hz}$, 200 K, 0.1 dex and 0.1 dex respectively. The number of models selected with these criteria ranged from about 80 to 800. For each of these models, the acoustic depths τ_{BCZ} and τ_{HeIIz} were determined by a procedure exactly similar to method B adopted for the real data. The theoretically computed value of the frequency was taken as the mean value and the uncertainty was adopted as that of the corresponding mode frequency in the *Kepler* data of the concerned star. Thus, the model data set mimicked the observed data set in terms of number of modes, specific modes used in the fitting and the error bars on the frequencies.

The comparison of the fractional acoustic radii of the glitches in the models and our estimates from the *Kepler* data are shown in Fig. 7 for two of the stars in our sample. One of them (KIC010963065) is a main-sequence star, while the other (KIC011244118) is in the sub-giant phase. In this figure we show the fractional acoustic radii of the glitches estimated from the *Kepler* data by method B along with the values obtained from the frequencies of the models by the same method, as described above. For the latter, the typical uncertainty (not shown in the graphs for the sake of clarity) would be similar to that of the values obtained from the *Kepler* data, since we have assumed the same uncertainties on the theoretical frequencies as the data. The acoustic depths obtained from the oscillatory signals have been converted to acoustic radii through the relation $t = T_0 - \tau \approx (2\Delta_0)^{-1} - \tau$. The error bars on the values from these methods include the uncertainty propagated in the calculation of T_0 from Δ_0 , as listed in Ta-

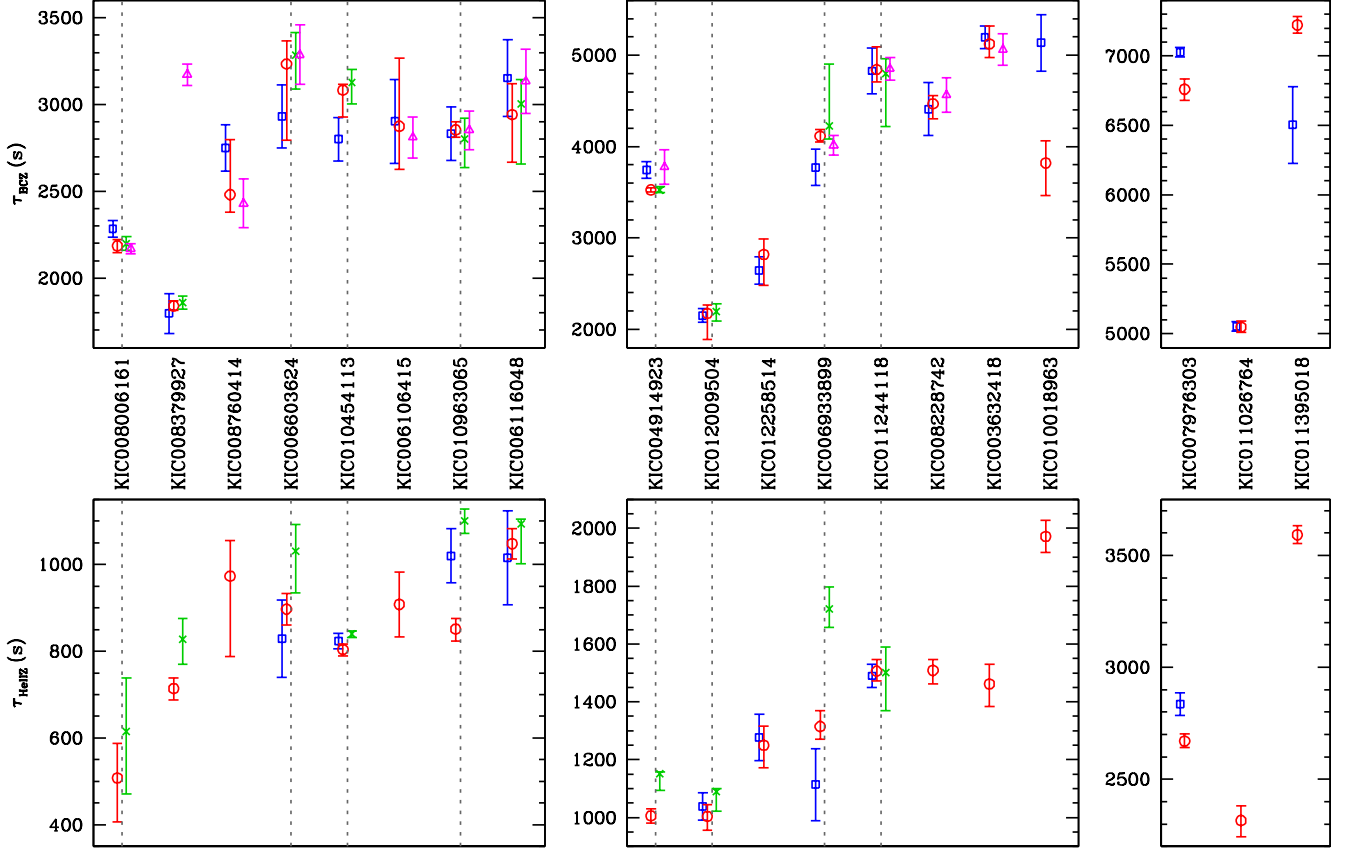


FIG. 6.— Comparison of acoustic depths τ_{BCZ} (upper panels) and τ_{HeIIZ} (lower panels) determined from the oscillatory signal in the *Kepler* frequencies of 19 stars by the four methods (blue empty squares for A, red empty circles for B, green crosses for C, and magenta empty triangles for D). The stars have been grouped in three graphs for each glitch with different ranges according to their estimated values of τ_{BCZ} and τ_{HeIIZ} . The values from different methods for each star are slightly offset along the horizontal direction from the central positions for clarity. The grey dotted lines indicate the selected set of eight stars for which results are shown in Figs. 2 to 5.

ble 2. The figure also shows the theoretical values of the fractional acoustic radii of the glitches from the models calculated using Eqs. (3) and (5). The two illustrated stars are typical of the sample. Results for others stars are similar to these with the discrepancies between the models and observations being either smaller or higher in a couple of stars.

4.2. Optimally fitted models

We also compared our estimated acoustic locations of the glitches to those in an optimally fitted model of each star. The fitted model was obtained through the Asteroseismic Modeling Portal (AMP, Metcalfe et al. 2009). The details of the stars studied here can be found in Mathur et al. (2012). Briefly, the models were obtained by optimizing the match between the observed frequencies and the modelled ones. To overcome the issue of the surface effects, we applied the empirical formula of Kjeldsen et al. (2008). The model acoustic radii were calculated as per the definitions given in Eq. (3). The comparison of AMP model values of the fractional acoustic radii and those obtained from the four methods is shown in Fig. 8.

For three of the stars, KIC08006161, KIC006106415 and KIC12009504, independent optimized models were made by fitting frequency ratios as described by Silva Aguirre et al. (2011, 2013). These models were constructed with the GARSTEC code (Weiss & Schlattl 2008), and are also shown in Fig. 8.

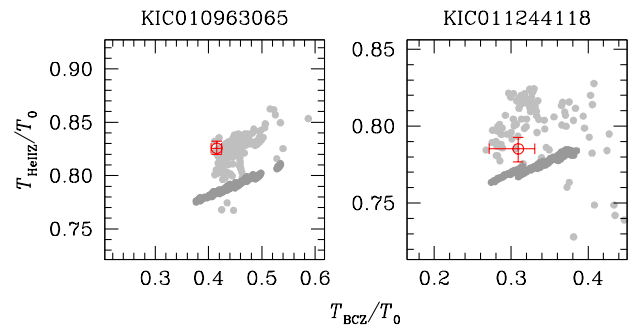


FIG. 7.— Comparison of fractional acoustic radii T_{BCZ}/T_0 and T_{HeIIZ}/T_0 determined from the oscillatory signal in the *Kepler* frequencies of 2 stars (KIC10963065 and KIC11244118) with corresponding values from representative models of the stars. In each case the red empty circle with error bars represents the results from the data while the light grey dots represent the values determined from the calculated frequencies of the models. Method B was employed in both cases. The dark grey dots indicate the actual values of the fractional acoustic radii in the stellar models, calculated using Eqs. (3) and (5). For each star, the ranges of each axis shown in the graph correspond to ± 1000 s and ± 500 s of the values of T_{BCZ} and T_{HeIIZ} determined from *Kepler* data, respectively.

5. DISCUSSION

5.1. Comparison between methods and uncertainties

Overall we find remarkably good agreement between the values of the acoustic depths of the BCZ determined by different methods. In most cases the τ_{BCZ} (or the corresponding

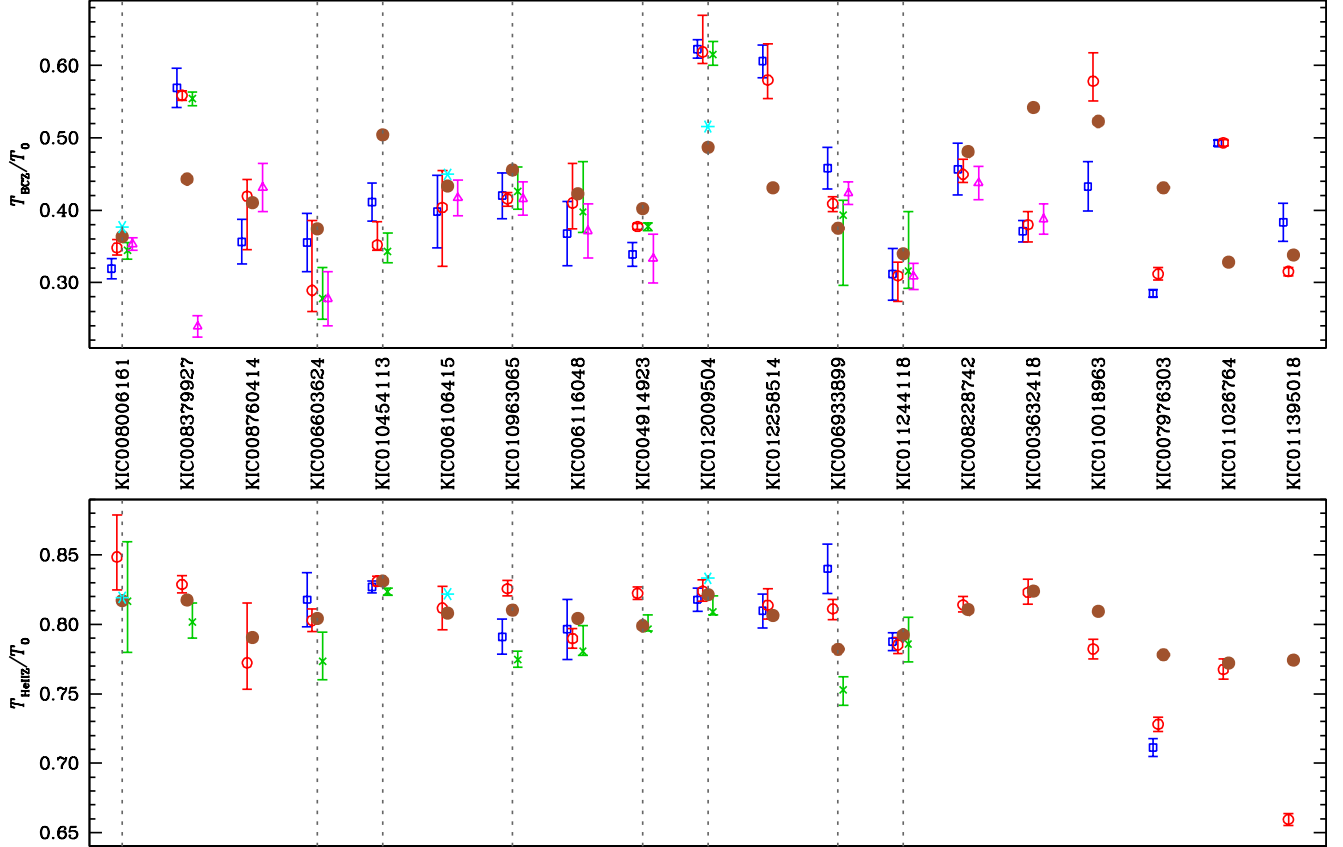


FIG. 8.— Comparison of fractional acoustic radii T_{BCZ}/T_0 and $T_{\text{HeII Z}}/T_0$ determined from the oscillatory signal in the *Kepler* frequencies of 19 stars by the four methods (blue empty squares for A, red empty circles for B, green crosses for C, and magenta empty triangles for D) and AMP model values (brown filled circles). For three stars values obtained from independently fitted models made by the GARSTEC code are also shown (cyan starred symbol). The values from different methods for each star are slightly offset along the horizontal direction from the central positions for clarity. The grey dotted lines indicate the selected set of eight stars for which results are shown in Figs. 2 to 5.

T_{BCZ}) agree with each other well within the quoted 1σ error bars (cf. Table 2 and Fig. 6). In terms of relative uncertainties, the τ_{BCZ} and $\tau_{\text{HeII Z}}$ values from different methods agree pairwise within 10% and 5%, respectively for most of the stars.

The general agreement between $\tau_{\text{HeII Z}}$ values from different methods is not as good as those for τ_{BCZ} , although it is mostly within 1σ uncertainties, and the values match always within 5% of each other, nevertheless. While comparing our estimates of the acoustic depths τ_{BCZ} and $\tau_{\text{HeII Z}}$ from methods A, B and C to the acoustic radii from method D, or from typical models, we invoked the relationship between the total acoustic radius T_0 and the average large separation Δ_0 , i.e., $T_0 \approx (2\Delta_0)^{-1}$. This relationship is an approximate one. Further, the observed average large separation, Δ_0 , depends on the adopted frequency range over which it is measured and also on the adopted method.

Particular attention should be paid to the systematic biases involved in treating the outermost layers of the star by different seismic diagnostics dealing with the determination of acoustic depths of glitches. Although one may hope that the different methods (seismic diagnostics) will provide similar stellar radii r for the acoustic glitches of both the helium ionization zones and the base of the surface convection zone, the seismically measured acoustic depths $\tau(r)$ of these glitches will in general be different, for they depend on the very details of the adopted seismic diagnostic. For example, method C approximates the outer stellar layers by a polytrope with a poly-

tropic index $m = 3.5$, allowing for some account of the location of the outer turning point of an incident acoustic wave by approximating the acoustic cutoff frequency $\nu_{\text{ac}} \simeq (m+1)/\tau$ (Houdek & Gough 2007). The location of the upper turning point affects the the phase of an incident mode and consequently also the location of the acoustic glitches, typically increasing their acoustic depths when the outer layers are approximated by a polytrope (Houdek & Gough 2007). A (mathematically) convenient way for estimating the phase at the upper turning point is to relate it to a fiducial location in the evanescent region far above the upper turning point, where the mode in the propagating region would “feel” the adiabatic sound speed c to vanish, i.e., where $c = 0$. This location, lying well inside the evanescent zone of most of the acoustic modes, defines the acoustic radius or acoustic surface. The squared adiabatic sound speed c^2 decreases in the adiabatically stratified region of an outer convection zone nearly linearly with radius (e.g. Balmforth & Gough 1990; Gough 2013). The location of the acoustic radius can therefore be estimated where the linearly outward extrapolated c^2 , with respect to radius r , vanishes. In a solar model the so-determined location of the seismic surface is about 111 s in acoustic height above the temperature minimum (Lopes & Gough 2001), or above 200 s in acoustic height above the photosphere (Monteiro et al. 1994; Houdek & Gough 2007). This shift may explain in part the differences between the location of the acoustic glitches between the stellar models and our seismically determined

values.

There is also a noticeable systematic shift between the acoustic depth of the HeIIZ in a stellar model and its value estimated from the oscillatory signal in the model frequencies (see Fig. 7). The fitted value of τ_{HeIIZ} , as obtained with methods A and B, is typically smaller than the model value by about 100 s, on average. However, we do not find such a systematic shift between the τ_{BCZ} values of the models and the fits. This is a general feature of most of the stars and might be because the depth of the HeII ionization zone cannot be uniquely defined since the ionization zone covers a finite range of radius. On the other hand, the base of the convection zone is a clearly defined layer within the star. Including also the glitch contribution from the first stage of helium ionization in the seismic diagnostic, additionally to the contribution from the second stage of helium ionization, perhaps leads to a more accurate definition of the acoustic depth of helium ionization, as considered in method C, resulting in larger values for the fitted acoustic depth τ_{HeIIZ} as indicated in Table 2.

In Table 2 and Figs. 7 and 8 we did not take account of these differences in the acoustic depths between the methods A, B and C and the calculated stellar models. It is also worth noticing that the T_0 values of AMP models are systematically smaller (by about 300 s, or, by about 4%, on average) than those estimated from Δ_0 of the *Kepler* data used in this paper (see Table 3). This may be due to a combination of factors, including imperfect modeling of the stars, especially of the surface layers. The AMP fitting has been subjected to the surface correction technique (Kjeldsen et al. 2008), while this was not included in the analysis of the present data. However, even with stellar models, a difference of up to 2% between the T_0 values derived from the asymptotic relation (Eq. (5)) and that from the large separation is expected (Hekker et al. 2013). Nevertheless, this contributes partially to the differences in the fractional acoustic radii of the glitches between AMP models and the estimates from the data. We have not estimated the uncertainties in the model values of the acoustic radii. Thus it is difficult to make any quantitative comparison between these values and those obtained from the data.

5.2. Discussion of specific stars

We discuss further the cases of the eight selected stars in detail below (ref. Figs. 2–5). The cases of the 11 remaining stars are somewhat similar to these and a general understanding of the issues involved may be obtained from the selected subsample itself.

5.2.1. KIC008006161

This is a low mass main sequence star and one of the easiest cases for the determination of τ_{BCZ} or T_{BCZ} , and all the methods converge to one consistent value which also agrees with the models. The determination of τ_{HeIIZ} from method A did not converge, and hence is not included. Methods B and C agree with the model values, as well as the AMP and GARSTEC values.

5.2.2. KIC006603624

The oscillatory signal from the BCZ for this star seems to be substantially weaker in comparison to the signal from the HeIIZ, as borne out in each of Figs. 2–5. In Fig. 2, the amplitude of the oscillations in $\delta\nu_{\text{BCZ}}$ does not exceed $0.1 \mu\text{Hz}$, lower than all the other stars shown. It is, therefore, somewhat difficult to determine the acoustic location of the BCZ. This

TABLE 3
ACOUSTIC RADII OF GLITCHES IN AMP MODELS.
TOTAL ACOUSTIC RADII OF THE STARS IN THE AMP
MODELS AND AS ESTIMATED FROM THE AVERAGE
LARGE SEPARATION ARE ALSO GIVEN.

KIC ID	T_{BCZ}^a (s)	T_{HeIIZ}^a (s)	T_0^a (s)	T_0^b (s)
KIC008006161*	1177	2647	3239	3353 ± 2
KIC008379927	1780	3285	4019	4170 ± 3
KIC008760414	1675	3229	4084	4273 ± 3
KIC006603624*	1629	3503	4356	4549 ± 4
KIC010454113*	2326	3832	4611	4757 ± 9
KIC006106415	2003	3735	4623	4821 ± 4
KIC010963065*	2128	3787	4673	4882 ± 4
KIC006116048	2019	3844	4779	4985 ± 9
KIC004914923*	2177	4322	5410	5662 ± 6
KIC012009504*	2660	4485	5461	5701 ± 6
KIC012258514	2761	5170	6410	6711 ± 9
KIC006933899*	2488	5188	6633	6963 ± 9
KIC011244118*	2286	5330	6726	7012 ± 19
KIC008228742	3724	6278	7746	8116 ± 13
KIC003632418	4289	6517	7911	8264 ± 13
KIC010018963	4516	6992	8640	9057 ± 32
KIC007976303	4012	7240	9305	9823 ± 38
KIC011026764	3103	7303	9459	9960 ± 19
KIC011395018	3363	7707	9954	10548 ± 22

^a Calculated from AMP model using Eqs. (3) and (5)

^b Estimated from Δ_0 of *Kepler* data

* Stars illustrated in Figs. 2–5.

is reflected in the wider and flatter peaks in the histogram in method B (see Fig. 3), the posterior probability distribution function (PDF) in method D (see Fig. 5), and the larger error bars from all the four methods. However, the median values of τ_{BCZ} derived from all the methods agree quite well. The values of τ_{HeIIZ} obtained from methods A and B agree with each other, but only at 2σ level with that from method C. The agreement with model values is barely at 1σ for T_{BCZ} but well within 1σ for T_{HeIIZ} . The AMP model is also consistent with the other models.

5.2.3. KIC010454113

This star was attempted by the first three methods, and they produce consistent results for both BCZ and HeIIZ. The model values also lie close to these. This case illustrates the problem of aliasing encountered while fitting the oscillatory signal due to BCZ (see Sect. A.2). This is reflected in the dual peaks in the histogram of method B (Fig. 3). Similarly, method C also finds a secondary value of τ_{BCZ} corresponding to the smaller peak from method B. We have considered the value with more number of Monte Carlo realisations as the true value of τ_{BCZ} .

5.2.4. KIC010963065

All the four methods provide almost identical determinations of τ_{BCZ} (or corresponding T_{BCZ}), but the τ_{HeIIZ} determined from method B agrees with those from the other two methods only at 2σ level. However, the model values span the range of the determined T_{HeIIZ} (cf. Figs. 7 and 8).

5.2.5. KIC004914923

The τ_{BCZ} values for this star have been obtained by all the methods, and the values agree within 1σ uncertainties. The PDF in method D shows a very small secondary peak at $T_{\text{BCZ}} \sim 3000$ s, but the histogram for τ_{BCZ} in method B shows no such feature. The τ_{HeIIZ} could not be determined from

method A, but both methods B and C provide values which agree within 2σ . The derived values for T_{BCZ} and T_{HeIIZ} agree quite well with those derived from the model frequencies, as well as the AMP model values.

5.2.6. KIC012009504

Three methods, A, B and C, were applied for this star. Although in method B we observed three peaks in the histogram for τ_{BCZ} , they cannot be explained as an aliasing artifact. Nevertheless, the highest peak value agrees very well with that from methods A and C. The τ_{HeIIZ} values obtained by the three methods also are consistent. However, the model values of T_{BCZ} , as derived from both AMP and GARSTEC models, seem to be smaller than our derived values, and actually correspond to the second highest peak in the histogram from method B. Given these facts, it is difficult to ascertain whether the discrepancy is because of inadequacy of the models to mimic the real star, or due to failure of our methods to detect the true oscillatory signal from the BCZ.

5.2.7. KIC006933899

The τ_{BCZ} values from all methods agree well within 1σ , as do the τ_{HeIIZ} determined from methods A and B. However, τ_{HeIIZ} from method C is more than 2σ deeper. While the model values of T_{BCZ} agree very well with all the derived values, the T_{HeIIZ} from methods A and B match the model fitted values while that from method C is close to the actual model value. The AMP model also lies in the vicinity of the other models.

5.2.8. KIC011244118

This is a relatively evolved star, for which there are possibly three mixed dipole modes. Once these modes are removed from consideration, all the four methods produce exceptionally close median values of both τ_{BCZ} (T_{BCZ}) and τ_{HeIIZ} (T_{HeIIZ}), even though the uncertainties are large in the former. The model fitted values have a larger scatter possibly because the radial orders of the mixed modes were not identical in such a wide range of models, and thus those were not all removed during fitting.

5.2.9. Other discrepant cases

For the remaining 11 stars in the sample, the four methods agree remarkably well for most cases. Some discrepancies do occur for KIC008379927, KIC010018963, KIC007976303, and KIC011395018.

For KIC008379927, the first three methods produce consistent results for τ_{BCZ} . Method D does produce a pronounced peak in the PDF, but at a value which is unlikely to correspond to the location of BCZ. A determination of τ_{HeIIZ} for this star was only possible from methods B and C which agree to within 1.5σ .

KIC010018963 seems to be a case where methods A and B have determined the mutually aliased values of τ_{BCZ} , and it is difficult to choose one over the other as the likely correct location of the BCZ.

KIC007976303 is an evolved star for which 23 frequencies could be used, and even some of these modes could be mixed in nature. Neither the τ_{BCZ} nor the τ_{HeIIZ} values determined from methods A and B agree for this star.

KIC011395018 is a sub-giant star with several mixed modes, and it is therefore hardly surprising that methods A and B have failed to produce consistent values of τ_{BCZ} .

6. SUMMARY

We have used the oscillatory signal in the frequencies of 19 *Kepler* stars to determine the location of the two major acoustic glitches in the stellar interior, namely, the base of the convection zone and the second helium ionization zone. Four independent approaches were used which exploited either the presence of the signal in the frequencies themselves, the second differences of the frequencies or the ratio of small to the large separation. For the stars where more than one method was applied, we found remarkable agreement in the results, in general. There were, however, a few discrepant cases, some of which could be traced to the issue of aliasing between the acoustic depth and radius of the glitch. In some others, the presence of mixed modes prevented an accurate analysis.

As a check on the values of the acoustic radii of the acoustic glitches determined from the observed frequencies of a star, we also compared them with theoretical model values. For each star, a large number of representative models were constructed and the same method applied for the theoretical frequencies of these as was done for the observed frequencies. For most of the stars the estimated location of the glitches were found to be in close agreement with the model values, within error bars.

Although these results confirm the validity of the analysis done, the major result of the present work is to open the possibility of using the parameters of the glitches to perform model fitting. The proposed approach adds additional observational constraints, independent from other global and seismic parameters, that can be used in the process of finding the best possible model that reproduces the observations. Most important, these additional constraints can be the source for studying necessary improvements in the physics in order to ensure that all observables are fitted, as has been done for the Sun already (e.g., Christensen-Dalsgaard et al. 2011; Houdek & Gough 2011).

The present work demonstrates the viability of the techniques applied to determine the acoustic location of layers of sharp variation of sound speed in the stellar interior. These methods thus provide powerful tools for placing constraints on the stratification inside solar-type stars (Monteiro et al. 2002; Mazumdar 2005). With the availability of precise frequency sets for a large number of stars from the *Kepler* mission, one can use these techniques to follow the variation of the locations of acoustic glitches in a large ensemble of solar-type stars populating the main sequence and sub-giant branches.

The amplitudes of the oscillatory signals from the acoustic glitches can also provide useful information about the stellar interior. The location as well as the strength of the glitch at the base of the convective envelope in cool stars can place independent constraints on the theories of convection (e.g. Christensen-Dalsgaard et al. 2011). Further, the amplitude of the oscillatory signal due to the second helium ionization zone can provide an estimate of the helium content in the stellar envelope (Pérez Hernández & Christensen-Dalsgaard 1998; Miglio et al. 2003; Basu et al. 2004; Monteiro & Thompson 2005; Houdek & Gough 2007).

We have demonstrated that the ratio τ_{BCZ}/T_0 can be determined to an accuracy of a few percent. This ratio can be used to constrain Z and hence may be able to distinguish between different heavy element mixtures. van Saders & Pinsonneault (2012) have estimated that a variation in heavy element abundances by 0.1 dex can shift the acoustic depth by about 1%

of the acoustic radius. Thus with improved data from *Kepler* it should be possible to achieve the required accuracy to distinguish between different heavy element mixtures. There could be other effects which may also shift the acoustic depth of the convection zone and these systematic effects need to be studied before we can use asteroseismic data to study Z . Nevertheless, the variation in τ_{BCZ} that we find is consistent with those of van Saders & Pinsonneault (2012). In view of the large uncertainty in $[\text{Fe}/\text{H}]$ and other stellar parameters it is difficult to make a direct comparison with the predictions of van Saders & Pinsonneault (2012).

The analyses carried out here have obviously provided estimates of the amplitudes and other properties of the fits. The manner in which these reflect the stellar properties depends sensitively on the details of the fitting techniques and hence, unlike the acoustic locations, a direct comparison of those results of the different techniques is not meaningful. The interpretation of the results in terms of stellar properties will require detailed comparisons with the results of analysis of stellar model data, to be carried out individually for each technique. Such studies are envisaged as a follow-up to the present work.

Funding for the *Kepler* Discovery mission is provided by NASA's Science Mission Directorate. AM acknowl-

edges support from the National Initiative on Undergraduate Science (NIUS) programme of HBCSE (TIFR). SB acknowledges support from NSF grant AST-1105930. GH acknowledges support by the Austrian Science Fund (FWF) project P21205-N16. MC and MJPFM acknowledge financial support from FCT/MCTES, Portugal, through the project PTDC/CTE-AST/098754/2008. MC is partially funded by POPH/FSE (EC). VSA received financial support from the *Excellence cluster "Origin and Structure of the Universe"* (Garching). DS acknowledges the financial support from CNES. Funding for the Stellar Astrophysics Centre is provided by The Danish National Research Foundation. The research is supported by the ASTERISK project (ASTERoseismic Investigations with SONG and *Kepler*) funded by the European Research Council (grant agreement no.: 267864). NCAR is partially supported by the National Science Foundation. This work was partially supported by the NASA grant NNX12AE17G. This work has been supported, in part, by the European Commission under SPACEINN (grant agreement FP7-SPACE-2012-312844). JB acknowledges Othman Benomar for useful advice on MCMC methods. We thank Tim Bedding for suggesting improvements to the manuscript. We thank the anonymous referee for helping us to improve the paper.

APPENDIX

METHODS FOR FITTING THE GLITCHES

We applied four different methods (labelled A to D) to determine the acoustic locations of the base of the convective zone (BCZ) and the second helium ionization zone (HeIIZ). Detailed descriptions of these methods are given in the following sections. In Figs. 2 to 5, we illustrate each of the four methods, as applied to some *Kepler* stars.

Method A

In this method the strategy is to isolate the signature of the acoustic glitches in the frequencies themselves. Compared to the methods involving second differences, described in Sects. A.2 and A.3, this has a different sensitivity to uncertainties (for a discussion on how the errors propagate, in comparison with the uncertainties, when using frequency combinations, please see the works by Ballot et al. 2004; Houdek & Gough 2007), does not require having frequencies of consecutive order and avoids the additional terms that need to be considered when fitting the expression to frequency differences. However, it is less robust on the convergence to a valid solution (the starting guess must be sufficiently close to the solution), since we do not put any constraints on what we consider to be a smooth component of the frequencies.

Here we assume that only very low-degree data are available so that any dependence of the oscillatory signal on mode degree can be ignored. The expression for the signature due to the BCZ is taken from Monteiro et al. (1994), Christensen-Dalsgaard et al. (1995), and Monteiro et al. (2000). The expression for the signature due to the HeIIZ is from Monteiro & Thompson (1998) and Monteiro & Thompson (2005), with some minor adaptations and/or simplifications.

In the following ν_r is a reference frequency, introduced for normalizing the amplitude. One good option would be to use $\nu_r = \nu_{\text{max}}$ (frequency of maximum power), but the actual value selected is not relevant unless we want to compare the amplitude of the signal of different stars.

The signal from the BCZ, after removing a smooth component from the frequencies, is written as (assuming there is no discontinuity in the temperature gradient at the BCZ)

$$\delta\nu_{\text{BCZ}} \simeq A_{\text{BCZ}} \left(\frac{\nu_r}{\nu}\right)^2 \sin(4\pi\tau_{\text{BCZ}}\nu + 2\phi_{\text{BCZ}}). \quad (\text{A1})$$

The parameters to be determined in this expression are A_{BCZ} , τ_{BCZ} , ϕ_{BCZ} for amplitude, acoustic depth and phase, respectively. The typical values to expect for a star like the Sun are $A_{\text{BCZ}} \sim 0.1 \mu\text{Hz}$, $\tau_{\text{BCZ}} \sim 2300 \text{ s}$ and $\phi_{\text{BCZ}} \sim \pi/4$.

The signal from HeIIZ, after removing a smooth component from the frequencies, is described by

$$\delta\nu_{\text{HeIIZ}} \simeq A_{\text{HeIIZ}} \left(\frac{\nu_r}{\nu}\right) \sin^2(2\pi\beta_{\text{HeIIZ}}\nu) \times \cos(4\pi\tau_{\text{HeIIZ}}\nu + 2\phi_{\text{HeIIZ}}). \quad (\text{A2})$$

The free parameters in this expression are A_{HeIIZ} , β_{HeIIZ} , τ_{HeIIZ} , ϕ_{HeIIZ} corresponding, respectively, to amplitude, acoustic width, acoustic depth and phase. The typical values to expect for a solar-like star for these parameters are $A_{\text{HeIIZ}} \sim 1.0 \mu\text{Hz}$, $\beta_{\text{HeIIZ}} \sim$

130 s, $\tau_{\text{HeIIZ}} \sim 700$ s and $\phi_{\text{HeIIZ}} \sim \pi/4$. When performing the fitting of Eq. (A2), leading to these parameters, it must be noted that the signature described by Eq. (A1) is ignored, being treated as noise in the residuals.

If low-degree frequencies are used for a solar-type star, then the signals present in the data correspond to having,

$$\nu = \nu_{s1} + \delta\nu_{\text{BCZ}} \quad (\text{A3})$$

or

$$\nu = \nu_{s2} + \delta\nu_{\text{HeIIZ}}. \quad (\text{A4})$$

Here ν_{si} ($i = 1, 2$) represents a ‘‘smooth’’ component of the mode frequency to be removed in the fitting. The parameters to fit these expressions are for Eq. (A1) (BCZ): A_{BCZ} , τ_{BCZ} , ϕ_{BCZ} ; and for Eq. (A2) (HeIIZ): A_{HeIIZ} , β_{HeIIZ} , τ_{HeIIZ} , ϕ_{HeIIZ} . In this case we treat $\delta\nu_{\text{BCZ}}$ as noise, since ν_{s2} is treated as including ν_{s1} and $\delta\nu_{\text{BCZ}}$.

The fitting procedure used is the same method as described by Monteiro et al. (2000). This method uses an iterative process in order to remove the slowly varying trend of the frequencies, leaving the required signature given in either Eq. (A1) or Eq. (A2). A polynomial in n was fitted to the frequencies of all modes of given degree l separately, using a regularized least-squares fit with third-derivative smoothing through a parameter λ_0 (see Monteiro et al. (1994) for the details). The residuals to those fits were then fitted for all degrees simultaneously. The latter fit is the ‘‘signal’’ either from the BCZ or from the HeIIZ. This procedure was then iterated (by decreasing the smoothing): at each iteration we removed from the frequencies the previously fitted signal and recalculated the smooth component of the frequencies, this time using the smaller value of λ_j ($j = 1, 2, 3, \dots$). The iteration converged when the relative changes to the smooth component of the signal fell below 10^{-6} (typically this happened for $j \simeq 3$).

The initial smoothing, selected through the parameter λ_0 , defines the range of wavelengths whose variation we want to isolate. To isolate the signature from the BCZ, a smaller initial value of λ_0 was required in order to ensure that the smooth component also extracts the signature from the HeIIZ. However, when isolating the signature from the HeIIZ, the shorter wavelength signature from the BCZ was also retained. We show the fits to Eqs. (A1) and (A2) in Fig. 2 for six of the *Kepler* stars that we studied.

In order to estimate the impact on the fitting of the observational uncertainties we used Monte Carlo simulations. We did so by producing sets of frequencies calculated from the observed values with added random values calculated from a standard normal distribution multiplied by the quoted observational uncertainty. In the fit we removed frequencies with large uncertainties ($> 0.5 \mu\text{Hz}$ for the BCZ and $> 1.0 \mu\text{Hz}$ for the HeIIZ). For each star we produced 500 sets of frequencies, determining the parameters as the standard deviation of the results for the parameters. Only valid fits were used, as long as the number of valid fits represented more than 90% of the simulations. Otherwise we considered that the signature had not been fit successfully (even if a solution could be found for the observations).

Method B

This method involves the second differences of the frequencies to determine τ_{BCZ} and τ_{HeIIZ} simultaneously by fitting a functional form to the oscillatory signals.

The oscillatory signal in the frequencies due to an acoustic glitch is quite small and is embedded in the frequencies together with a smooth trend arising from the regular variation of the sound speed in the stellar interior. It can be enhanced by using the second differences

$$\Delta_2\nu(n, l) = \nu(n-1, l) - 2\nu(n, l) + \nu(n+1, l), \quad (\text{A5})$$

instead of the frequencies $\nu(n, l)$ themselves (see, e.g., Gough 1990; Basu et al. 1994; Mazumdar & Antia 2001; Basu et al. 2004).

We fitted the second differences to a suitable function representing the oscillatory signals from the two acoustic glitches (Mazumdar & Antia 2001). We used the following functional form which has been adapted from Houdek & Gough (2007) (Eq. (22) therein):

$$\begin{aligned} \Delta_2\nu = & a_0 \\ & + \frac{b_2}{\nu^2} \sin(4\pi\nu\tau_{\text{BCZ}} + 2\phi_{\text{BCZ}}) \\ & + c_0\nu e^{-c_2\nu^2} \sin(4\pi\nu\tau_{\text{HeIIZ}} + 2\phi_{\text{HeIIZ}}), \end{aligned} \quad (\text{A6})$$

where a_0 , b_2 , c_0 , c_2 , τ_{BCZ} , ϕ_{BCZ} , τ_{HeIIZ} and ϕ_{HeIIZ} are 8 free parameters of fitting. For one of the stars in our set (KIC010018963), we needed to use a slightly different function in which the constant term representing the smooth trend, a_0 , was replaced by a parabolic form: $(a_0 + a_1\nu + a_2\nu^2)$. This was necessitated by the sensitivity of the fitted τ values to small perturbations to the input frequencies. The two τ values for the BCZ and the HeIIZ had about 10 times larger (and overlapping) uncertainties with the constant form, as compared to those with the parabolic form. Although this parabolic form could, in principle, be used for all stars as well, it actually interferes with the slowly varying periodic HeIIZ component in the limited range of observed frequencies, and makes it difficult to determine τ_{HeIIZ} . Therefore, in adopting Eq. (A6) we essentially assumed that the smooth trend in the frequencies had been reduced to a constant shift in the process of taking the second differences. We ignored frequencies which have uncertainties of more than $1 \mu\text{Hz}$.

While Eq. (A6) is not the exact form prescribed by Houdek & Gough (2007), it captures the essential elements of that form while keeping the number of free parameters relatively small. The ignored terms can be shown to have relatively smaller contributions. We note that Basu et al. (2004) have shown that the exact form of the amplitudes of the oscillatory signal does not affect the results significantly (however, see also Houdek & Gough 2006). The fits of Eq. (A6) to the second differences of some selected stars in our sample are shown in the *left* panels of Fig. 3.

The fitting procedure is similar to the one described by Mazumdar et al. (2012). The fit was carried out through a nonlinear χ^2 minimization, weighted by the uncertainties in the data. The correlation of uncertainties in the second differences was accounted for by defining the χ^2 using a covariance matrix. The effects of the uncertainties were considered by repeating the fit for 1000 realizations of the data, produced by perturbing the frequencies by random uncertainties corresponding to a normal distribution with standard deviation equal to the quoted 1σ uncertainty in the frequencies. The successful convergence of such a non-linear fitting procedure is somewhat dependent on the choice of reasonable initial guesses. To remove the effect of initial guesses affecting the final fitted parameters, we carried out the fit for multiple combinations of starting values. For each realization, the fitting was repeated for 100 random combinations of initial guesses of the free parameters and the fit which produced the minimum value of χ^2 was accepted.

The median value of each parameter for 1000 realizations was taken as its fitted value. The $\pm 1\sigma$ uncertainty in the parameter was estimated from the range of values covering 34% area about the median in the histogram of fitted values, assuming the error distribution to be Gaussian. Thus the quoted uncertainties in these parameters reflect the width of these histograms on two sides of the median value. The histograms for τ_{BCZ} and τ_{HeIIZ} and the ranges of initial guesses of the corresponding parameters are shown in the *right* panels of Fig. 3.

In some cases the fitting of the τ_{BCZ} parameter suffers from the aliasing problem (Mazumdar & Antia 2001), where a significant fraction of the realizations are fitted with τ_{BCZ} equal to $\tilde{\tau}_{\text{BCZ}} \equiv T_0 - \tau_{\text{BCZ}}$. This becomes apparent from the histogram of τ_{BCZ} which appears bimodal with a reflection around $T_0/2$ (e.g., for KIC010454113, shown in Fig. 3). In such cases, we chose the higher peak in the histogram to represent the true value of τ_{BCZ} , and the uncertainty in the parameter was calculated after ‘‘folding’’ the histogram about the acoustic mid-point $T_0/2$, the acoustic radius being estimated from the mean large separation, Δ_0 . For a few stars there are multiple peaks in the histogram for τ_{BCZ} , not all of which can be associated with the true depth of the BCZ or its aliased value (e.g., for KIC012009504, shown in *bottom right* panel of Fig. 3). In such cases we chose only the most prominent peak to determine the median and the uncertainty was estimated from the width of that peak. The remaining realizations were also neglected for estimating the other parameters such as τ_{HeIIZ} .

Method C

Approximate expressions for the frequency contributions $\delta\nu_i$ arising from acoustic glitches in solar-type stars were recently presented by Houdek & Gough (2007, 2011), which we adopt here for producing the results presented in Fig. 4 and Table 2. A detailed discussion of the method can be found in those references; we therefore present here only a summary. The complete expression for $\delta\nu_i$ is given by

$$\delta\nu_i = \delta_\gamma\nu_i + \delta_c\nu_i + \delta_u\nu_i, \quad (\text{A7})$$

where the terms on the RHS are the individual acoustic glitch components located at different depths inside the star.

The first component,

$$\begin{aligned} \delta_\gamma\nu = & -\sqrt{2\pi}A_{\text{II}}\Delta_{\text{II}}^{-1} \left[\nu + \frac{1}{2}(m+1)\Delta_0 \right] \\ & \times \left[\tilde{\beta} \int_0^{T_0} \kappa^{-1} e^{-\frac{(\tau-\tilde{\eta}\tau_{\text{II}})^2}{2\tilde{\mu}^2\Delta_{\text{II}}^2}} |x|^{1/2} |\text{Ai}(-x)|^2 d\tau \right. \\ & \left. + \int_0^{T_0} \kappa^{-1} e^{-\frac{(\tau-\tau_{\text{II}})^2}{2\Delta_{\text{II}}^2}} |x|^{1/2} |\text{Ai}(-x)|^2 d\tau \right] \end{aligned} \quad (\text{A8})$$

arises from the variation in γ_1 induced by helium ionization. The constant $m = 3.5$ is a representative polytropic index in the expression for the approximate effective phase ψ appearing in the argument $x = \text{sgn}(\psi)|3\psi/2|^{2/3}$ of the Airy function $\text{Ai}(-x)$. We approximate ψ as

$$\psi(\tau) = \kappa\omega\tilde{\tau} - (m+1)\cos^{-1}[(m+1)/\omega\tilde{\tau}], \quad (\text{A9})$$

if $\tilde{\tau} > \tau_t$, and

$$\psi(\tau) = |\kappa|\omega\tilde{\tau} - (m+1)\ln[(m+1)/\omega\tilde{\tau} + |\kappa|], \quad (\text{A10})$$

if $\tilde{\tau} \leq \tau_t$, in which $\tilde{\tau} = \tau + \omega^{-1}\epsilon_{\text{II}}$, with ϵ_{II} ($\epsilon_1 = \epsilon_{\text{II}}$) being a phase constant, and τ_t is the location of the upper turning point of the mode. The location of the upper turning point of the oscillation mode is determined approximately from the polytropic representation of the acoustic cutoff frequency, leading to the expressions $\kappa(\tau) = [1 - (m+1)^2/\omega^2\tilde{\tau}^2]^{1/2}$.

The coefficients associated with the glitch contribution from the first stage of helium ionization (He I) (first integral expression in Eq. (A8)) are related to the coefficients of the second stage of helium ionization (He II) by the constant ratios $\tilde{\beta} := A_{\text{I}}\Delta_{\text{II}}/A_{\text{II}}\Delta_{\text{I}}$, $\tilde{\eta} := \tau_{\text{I}}/\tau_{\text{II}}$ and $\tilde{\mu} := \Delta_{\text{I}}/\Delta_{\text{II}}$, where A_{II} is the amplitude factor of the oscillatory He II glitch component, Δ_{II} is the acoustic width of the glitch and $\tau_{\text{II}} \equiv \tau_{\text{HeIIZ}}$ is its acoustic depth beneath the seismic surface. For the constant ratios $\tilde{\beta}$, $\tilde{\eta}$, and $\tilde{\mu}$ we set the values 0.45, 0.70 and 0.90, respectively, as did Houdek & Gough (2007, 2011). With this approach the addition of the He I contribution does not introduce additional fitting coefficients in the seismic diagnostic (A8).

The second component in Eq. (A7),

$$\begin{aligned} \delta_c\nu \simeq & A_c\Delta_0^3\nu^{-2} (1 + 1/16\pi^2\tau_0^2\nu^2)^{-1/2} \\ & \times \left\{ \cos[2\psi_c + \tan^{-1}(4\pi\tau_0\nu)] \right. \\ & \left. - (16\pi^2\tilde{\tau}_{\text{BCZ}}^2\nu^2 + 1)^{1/2} \right\} \end{aligned} \quad (\text{A11})$$

arises from the acoustic glitch at the base of the convection zone resulting from a near discontinuity (a true discontinuity in theoretical models using local mixing length theory with a non-zero mixing length at the lower boundary of the convection zone) in the second derivative of density. We model this acoustic glitch with a discontinuity in the squared acoustic cutoff frequency ω_c^2 at τ_{BCZ} , with A_c being proportional to the jump in ω_c^2 , coupled with an exponential relaxation to a putative, glitch-free, model in the radiative zone beneath, with a relaxation time scale $\tau_0 = 80$ s, as did Houdek & Gough (2007, 2011). This leads to

$$\begin{aligned} \psi_c = & \kappa_c \omega \tilde{\tau}_{\text{BCZ}} \\ & - (m+1) \cos^{-1} [(m+1)/\tilde{\tau}_{\text{BCZ}}\omega] \\ & + \pi/4, \end{aligned} \quad (\text{A12})$$

where $\kappa_c = \kappa(\tau_{\text{BCZ}})$ and $\tilde{\tau}_{\text{BCZ}} = \tau_{\text{BCZ}} + \omega^{-1} \epsilon_c$ with ϵ_c being a constant phase.

The additional upper-glitch component $\delta_u \nu_i$ (i enumerates individual frequencies), which is produced, in part, by wave refraction in the stellar core, by the ionization of hydrogen and by the upper superadiabatic boundary layer of the envelope convection zone, is difficult to model. We approximate its contribution to $\Delta_2 \nu$ as a series of inverse powers of ν , truncated at the cubic order:

$$\Delta_2 \delta_u \nu_i = \sum_{k=0}^3 a_k \nu_i^{-k}. \quad (\text{A13})$$

The eleven coefficients $\eta_\alpha = (A_{\text{II}}, \Delta_{\text{II}}, \tau_{\text{HeIIZ}}, \epsilon_{\text{II}}, A_c, \tau_{\text{BCZ}}, \epsilon_c, a_0, a_1, a_2, a_3)$, $\alpha = 1, \dots, 11$, were found by fitting the second differences (cf. Eq. (A5)),

$$\begin{aligned} \Delta_{2i} \nu(n, l) & := \nu(n-1, l) - 2\nu(n, l) + \nu(n+1, l) \\ & \simeq \Delta_{2i}(\delta_\gamma \nu + \delta_c \nu + \delta_u \nu) =: g_i(\nu_j; \eta_\alpha) \end{aligned} \quad (\text{A14})$$

to the corresponding observations by minimizing

$$E_g = \sum_{i,j} (\Delta_{2i} \nu - g_i) C_{\Delta ij}^{-1} (\Delta_{2j} \nu - g_j), \quad (\text{A15})$$

where $C_{\Delta ij}^{-1}$ is the (i, j) element of the inverse of the covariance matrix C_Δ of the observational uncertainties in $\Delta_{2i} \nu$, computed, perforce, under the assumption that the uncertainties in the frequency data ν_i are independent. The covariance matrix $C_{\eta_\alpha \gamma}$ of the uncertainties in the fitting coefficients η_α were established by Monte Carlo simulation.

Results for six of the stars in our sample are shown in Fig. 4 in which also the individual acoustic glitch contributions are illustrated in the *lower* panels.

Method D

Determinations of acoustic depths of glitches are biased by surface effects (e.g. Christensen-Dalsgaard et al. 1995). A way to remove such biases is to consider acoustic radii of the signatures. First, it is possible to perform posterior determinations of radii by comparing depths to the total acoustic radius of the star derived from the average large separation Δ_0 (see Ballot et al. 2004); it is also possible to directly measure acoustic radii by considering the small separations d_{01} and d_{10} or the frequency ratios r_{01} and r_{10} as shown by Roxburgh & Vorontsov (2003).

We use the 3-point differences:

$$d_{01,n} = \frac{1}{2}(2\nu_{n,0} - \nu_{n-1,1} - \nu_{n,1}), \quad (\text{A16})$$

$$d_{10,n} = -\frac{1}{2}(2\nu_{n,1} - \nu_{n,0} - \nu_{n+1,0}) \quad (\text{A17})$$

and the corresponding ratios:

$$r_{01,n} = \frac{d_{01,n}}{\Delta \nu_{1,n}}, r_{10,n} = \frac{d_{10,n}}{\Delta \nu_{0,n+1}}. \quad (\text{A18})$$

We denote by d_{010} and r_{010} the sets $\{d_{01}, d_{10}\}$ and $\{r_{01}, r_{10}\}$, respectively.

Using these variables, the main contributions of outer layers are removed (see Roxburgh 2005). The global trend of these variables then gives information on the core of the star (e.g. Silva Aguirre et al. 2011; Cunha & Brandão 2011). Nevertheless, the most internal glitches, such as the BCZ, also imprint their signatures over the global trend. Using solar data, Roxburgh (2009) showed that we can recover the acoustic radius of the BCZ (T_{BCZ}) by the use of a Fourier transform on the residuals obtained after removing the global trend. As a consequence of this approach, information about surface layers, including He I and He II ionization zones, are lost.

We used an approach similar to Roxburgh (2009) and develop a semi-automatic pipeline which extracts glitches from a frequency table of $l = 0$ and 1 modes. Instead of fitting a background first, then making a Fourier transform, we do both simultaneously by fitting the variable $y = \nu^* r_{010}$ (or $y = \nu^* d_{010}$) with the following expression:

$$f(\nu) = \sum_{k=0}^m \frac{c_k}{(\nu + \nu_\tau)^k} + A \sin(4\pi T \nu + \phi), \quad (\text{A19})$$

where $\nu^* = \nu/\nu_r$ and ν_r is a reference frequency. We have $m+3$ free parameters: $\{c_k\}$, A , T , and ϕ .

To be able to estimate reliable uncertainties for T_{BCZ} we performed a Markov Chain Monte Carlo (MCMC) to fit the data. Our MCMC fitting algorithm is close to the one described, for example, in Benomar et al. (2009) or Handberg & Campante (2011), but without parallel tempering. Moreover, in our case the noise is not multiplicative and exponential, but additive and normal. We fixed $m=2$ and $\nu_r = 0.8\nu_{\text{max}}$, similar to the value adopted for the Sun by Roxburgh (2009). We used uniform priors for A , T and ϕ . The prior for A was very broad (between 0 and $10\max(|y|)$); ϕ was 2π -periodic with a uniform prior over $[0, 2\pi]$, and T was restricted to $[\delta T, T_0 - \delta T]$, where $\delta T = (\max(\nu) - \min(\nu))^{-1}$. To determine priors for $\{c_k\}$, we first performed a standard linear least-square fitting without including the oscillatory component. Once we obtained the fitted values \tilde{c}_k and associated uncertainties σ_k , we used for c_k priors which are uniform over $[\tilde{c}_k - 3\sigma_k, \tilde{c}_k + 3\sigma_k]$ with Gaussian decay around this interval. After a 200 000-iteration learning phase (the learning method we used is based on Benomar et al. 2009), MCMC was run for 10^7 iterations. We tested the convergence by verifying the consistence of results obtained by using the first and second half of the chain.

Posterior probability distribution functions (PDF) for T are plotted for different stars in Fig. 5. Some PDFs exhibit a unique and clear mode that we attributed to the BCZ. T_{BCZ} was then estimated as the median of the distribution and 1σ error bars were taken as 68 % confidence limit of the PDF. Nevertheless, some other PDFs exhibit other small peaks. They can be due to noise, but they also can be due to other glitch signatures present in the data, especially tiny residuals from the outer layers. To take care of such situations, we also computed T_{BCZ} by isolating the highest peak and fitting it with a Gaussian profile. When the secondary peaks are small enough, the values and associated uncertainties obtained through the two methods are very similar. We have been successful mainly on main-sequence stars, while subgiant stars presenting mixed modes strongly disturb the analysis.

DETAILS OF YREC STELLAR MODELS

The input physics for the YREC models included the OPAL equation of state (Rogers & Nayfonov 2002) and the OPAL high-temperature opacities (Iglesias & Rogers 1996) supplemented with low-temperature opacities from Ferguson et al. (2005). All nuclear reaction rates were from Adelberger et al. (1998), except for the rate of the $^{14}\text{N}(p, \gamma)^{15}\text{O}$ reaction, which was fixed at the value of Formicola et al. (2004). Core overshoot of $0.2H_p$ was included where relevant. For the stars that did not have very low metallicities, we included the diffusion and settling of helium and heavy elements. This was done as per the prescription of Thoul et al. (1994).

We use four grids for this: the models from the Yonsei-Yale (YY) isochrones (Demarque et al. 2004), and the grids of Dotter et al. (2008), Marigo et al. (2008) and Gai et al. (2011).

REFERENCES

- Adelberger E. G., Austin, S. M., Bahcall, J. N., et al. 1998, *Rev. Mod. Phys.*, 70, 1265
- Appourchaux, T., Chaplin, W. J., García, R. A., et al. 2012, *A&A*, 543, A54
- Asplund, M., Grevesse, N., Sauval, A. J., & Scott, P. 2009, *ARA&A*, 47, 481
- Ballot, J., Turck-Chièze, S., & García, R. A. 2004, *A&A*, 423, 1051
- Balmforth N. J. & Gough D. O. 1990, *ApJ*, 362, 256
- Basu, S. 1997, *MNRAS*, 288, 572
- Basu, S., & Antia, H. M. 2008, *Phys. Rep.*, 457, 217
- Basu, S., Antia, H. M., & Narasimha, D. 1994, *MNRAS*, 267, 209
- Basu, S., Chaplin, W. J., Elsworth, Y. 2010, *ApJ*, 710, 1596
- Basu, S., Mazumdar, A., Antia, H. M., & Demarque, P. 2004, *MNRAS*, 350, 277
- Bedding, T. R., Kjeldsen, H., Campante, T. L., et al. 2010, *ApJ*, 713, 935
- Benomar, O., Appourchaux, T., & Baudin, F. 2009, *A&A*, 506, 15
- Borucki W. J. et al. 2010, *Sci*, 327, 977
- Bruntt, H., Basu, S., Smalley, B., et al. 2012, *MNRAS*, 423, 122
- Christensen-Dalsgaard, J., Monteiro, M. J. P. F. G., Thompson, M. J. 1995, *MNRAS*, 276, 283
- Christensen-Dalsgaard, J., Monteiro, M. J. P. F. G., Rempel, M., Thompson, M. J. 2011, *MNRAS*, 414, 1158
- Cunha, M. S., & Brandão, I. M. 2011, *A&A*, 529, A10
- Demarque, P., Woo, J.-H., Kim, Y.-C., & Yi, S. K. 2004, *ApJS*, 155, 667
- Demarque, P., Guenther, D. B., Li, L. H., Mazumdar, A., & Straka, C. W. 2008, *Ap&SS*, 316, 31
- Dotter, A., Chaboyer, B., Jevremovic, D. et al. 2008, *ApJ*, 178, 89
- Ferguson, J. W., Alexander, D. R., Allard, F., et al. 2005, *ApJ*, 623, 585
- Formicola A., Imbriani, G., Costantini, H. et al. 2004, *Physics Letters B*, 591, 61
- Gai, N., Basu, S., Chaplin, W. J., Elsworth, Y. 2011, *ApJ*, 730, 63
- García, R. A., Hekker, S., Stello, D., et al. 2011, *MNRAS*, 414, L6
- Gilliland, R. L., Jenkins, J. M., Borucki, W. J., et al. 2010, *ApJ*, 713, L160
- Gough D. O. 1986, in *Hydrodynamic and Magnetodynamic Problems in the Sun and Stars*. Y. Osaki, ed., Univ. Tokyo Press, 117
- Gough, D. O. 1990, *Progress of Seismology of the Sun and Stars*, 367, 283
- Gough D. O. 2002, in *Proceedings of the First Eddington Workshop on Stellar Structure and Habitable Planet Finding*. B. Battrick, F. Favata, I. W. Roxburgh & D. Galadi, eds., ESA SP-485, Noordwijk: ESA, p. 65
- Gough, D. 2013, *Sol. Phys.*, 287, 9
- Gough, D. O., & Sekii, T. 1993, in *GONG 1992: Seismic Investigation of the Sun and Stars*. T. M. Brown, ed., ASP Conf. Ser. Vol. 42., Astron. Soc. Pac., San Francisco, p. 177
- Gough, D. O., & Thompson, M. J. 1988, in *Advances in Helio- and Asteroseismology*. J. Christensen-Dalsgaard, S. Frandsen, eds., Reidel Publishing Company, 155
- Grevesse, N., & Sauval, A. J. 1998, *Space Sci. Rev.*, 85, 161
- Handberg, R., & Campante, T. L. 2011, *A&A*, 527, A56
- Hekker, S., Elsworth, Y., Basu, S., et al. 2013, accepted for publication in *MNRAS* (arXiv:1306.4323)
- Houdek, G. 2004, in *Equation-of-state and Phase-transition Issues in Models of Ordinary Astrophysical Matter*. V. Celebonovic, W. Däppen, D. O. Gough, eds., AIP Conf. Proc., Vol. 731, AIP, New York, p. 193
- Houdek, G., Gough, D. O. 2006, in *Proc. SOHO18/GONG 2006/HELAS I: Beyond the spherical Sun*. M. Thompson, K. Fletcher, eds., ESA SP-624, Noordwijk, p. 88
- Houdek, G., Gough, D. O. 2007, *MNRAS*, 375, 861
- Houdek, G., Gough, D. O. 2011, *MNRAS*, 418, 1217
- Iglesias, C. A., Rogers, F. J. 1996, *ApJ*, 464, 943
- Kjeldsen, H., Bedding, T. R., & Christensen-Dalsgaard, J. 2008, *ApJ*, 683, L175
- Koch D. G. et al. 2010, *ApJ*, 713, L79

- Lopes I. P. & Gough D. O. 2001, MNRAS, 322, 473
- Marigo, P., Girardi, L., Bressan, A. et al. 2008, A&A, 482, 883
- Mathur, S., Metcalfe, T. S., Woitaszek, M. et al. 2012, ApJ, 749, 152
- Mazumdar, A. 2005, A&A, 441, 1079
- Mazumdar, A., & Antia, H. M. 2001, A&A, 377, 192
- Mazumdar, A., Michel, E., Antia, H. M., Deheuvels, S. 2011, in Transiting planets, vibrating stars and their connection, Proceedings of the Second *CoRoT* Symposium. A. Baglin, M. Deleuil, E. Michel, C. Moutou & T. Seaman, eds., p. 197
- Mazumdar, A., Michel, E., Antia, H. M., Deheuvels, S. 2012, A&A, 540, A31
- Metcalfe, T. S., Creevey, O. L., & Christensen-Dalsgaard, J. 2009, ApJ, 699, 373
- Miglio A., Christensen-Dalsgaard J., di Mauro M. P., Monteiro M. J. P. F. G., Thompson M. J. 2003, in Asteroseismology Across the HR Diagram, Proceedings of the Asteroseismology Workshop, Porto, Portugal. M. J. Thompson, M. S. Cunha, M. J. P. F. G. Monteiro, eds., Kluwer Academic Publishers, Dordrecht, p. 537
- Miglio, A., Montalbán, J., Carrier, F., et al. 2010, A&A, 520, L6
- Monteiro, M. J. P. F. G., Christensen-Dalsgaard, J., Thompson, M. J. 1994, A&A, 283, 247
- Monteiro, M. J. P. F. G., Christensen-Dalsgaard, J., Thompson, M. J. 2000, MNRAS, 316, 165
- Monteiro, M. J. P. F. G., Christensen-Dalsgaard, J., Thompson, M. J. 2002, in Stellar Structure and Habitable Planet Finding. F. Favata, I. W. Roxburgh, D. Galadí-Enríquez, eds., ESA Publications Division, ESA SP-485, 291
- Monteiro, M. J. P. F. G., & Thompson, M. J. 1998, in Structure and Dynamics of the Interior of the Sun and Sun-like Stars. S. G. Korzennik, A. Wilson, eds., ESA Publications Division, ESA SP-418, 819
- Monteiro, M. J. P. F. G., & Thompson, M. J. 2005, MNRAS, 361, 1187
- Morel, P., & Lebreton, Y. 2008, Ap&SS, 316, 61
- Pérez Hernández, F., & Christensen-Dalsgaard, J. 1998, MNRAS, 295, 344
- Piau, L., Ballot, J., & Turck-Chièze, S. 2005, A&A, 430, 571
- Rogers, F. J., Nayfonov, A. 2002, ApJ, 576, 1064
- Roxburgh, I. W. 2005, A&A, 434, 665
- Roxburgh, I. W. 2009, A&A, 493, 185
- Roxburgh, I. W. 2011, in Transiting planets, vibrating stars and their connection, Proceedings of the Second *CoRoT* Symposium, A. Baglin, M. Deleuil, E. Michel, C. Moutou & T. Seaman, eds., p. 161
- Roxburgh, I. W. & Vorontsov, S. V. 1994, MNRAS, 268, 880
- Roxburgh, I. W. & Vorontsov, S. V. 2003, A&A, 411, 215
- Silva Aguirre, V., Ballot, J., Serenelli, A. M., & Weiss, A. 2011, A&A, 529, A63
- Silva Aguirre, V., Basu, S., Brandão, I. M., et al. 2013, ApJ, 769, 141
- Tassoul M. 1980, ApJS, 43, 469
- Thoul A. A., Bahcall J. N., Loeb A. 1994, ApJ, 421, 828
- Weiss, A., & Schlattl, H. 2008, Ap&SS, 316, 99
- van Saders, J. L., & Pinsonneault, M. H. 2012, ApJ, 746, 16
- Verner, G. A., Elsworth, Y., Chaplin, W. J., et al. 2011, MNRAS, 415, 3539
- Vorontsov, S. V. 1988, in Advances in Helio- and Asteroseismology. J. Christensen-Dalsgaard, S. Frandsen, eds., (Reidel), IAU Symp, 123, 151